



**Radiological impact of El Hierro
submarine volcano on the brown
algae *Lobophora variegata***

Neus Miquel i Armengol

Curso 2019/2020

Dra. Alicia M. Tejera Cruz

Dr. Pablo Martel Escobar

Dr. Fernando José Tuya Cortés

Trabajo de Fin de Título para la obtención del
título Máster Interuniversitario en Oceanografía

Radiological impact of El Hierro submarine volcano on the brown algae *Lobophora variegata*

Datos personales del estudiante

Neus Miquel i Armengol

Máster Interuniversitario de Oceanografía

Curso 2019/2020

Universidad de Las Palmas de Gran Canaria

Facultad de Ciencias del Mar

Datos de los tutores

Dra. Alicia M. Tejera Cruz

Universidad de Las Palmas de Gran Canaria

Facultad de Ciencias del Mar

Departamento de Física

Dr. Pablo Martel Escobar

Universidad de Las Palmas de Gran Canaria

Facultad de Ciencias del Mar

Departamento de Física

Dr. Fernando J. Tuya Cortés

Universidad de Las Palmas de Gran Canaria

Facultad de Ciencias del Mar

Departamento de Biología

En Las Palmas de Gran Canaria a 18 de septiembre de 2020

Table of Contents

Abstract	1
1. Introduction	2
1.1 Radioactivity in the marine environment	3
1.2 Use of radionuclides as tracers of marine environmental processes	4
2. Materials and methods	7
2.1. Sampling and sample preparation	7
2.2. Gamma and alpha spectrometry	9
2.2.1. Gamma spectrometry technique	9
2.2.2. Alpha spectrometry technique	10
2.3. Activity concentrations	13
2.4. Data analysis	13
2.4.1. Activity corrections	13
2.4.2. Statistical analysis	14
2.5. Performance criteria	14
3. Results and discussions	15
3.1. Radionuclides activity concentrations	15
3.2. Concentration factors	18
3.3 Uranium and Thorium series ratios	20
3.4 Statistical analysis	22
4. Conclusions	26
5. References	28
Annex I – Radioactive decay series	32
I.I. Natural radioactive decay series of ^{238}U	32
I.II Natural radioactive decay series of ^{232}Th	33
I.III. Natural radioactive decay series of ^{235}U	34
Annex II	35

Abstract

In this work, we present the radiological impact in the surroundings of the Tagoro submarine volcano several years after its eruptive analysing marine environmental samples. For this purpose, besides collecting coastal water, brown algae *Lobophora variegata* were collected along the coastal perimeter of El Hierro island, with the aim of using them as an environmental dosimeter due to their high accumulation power. Radionuclides analysed by alpha and gamma spectrometry were ^{238}U , ^{234}Th , ^{234}U , ^{226}Ra , ^{210}Pb , ^{210}Po , ^{235}U , ^{228}Th , and ^{40}K . The activity concentrations, concentration factors (CF) and ratios were calculated for all the samples taking into account the area affected by the volcano and the unaffected area. In the latter case, *L. variegata* algae collected on Las Canteras beach were also analysed. Lower values of activity concentrations for ^{234}Th and ^{234}U were measured in La Restinga zone (1310 ± 50 Bq/Kg; 5.8 ± 0.6 Bq/Kg) than ones obtained in the other areas non affected by the volcano (1660 ± 70 Bq/Kg; 7.5 ± 0.6 Bq/Kg); however, they were higher in El Hierro (1570 ± 60 Bq/Kg; 94 ± 8 Bq/Kg) than in Las Canteras (600 ± 30 Bq/Kg; 77 ± 8 Bq/Kg). Respect to coastal water samples, activity concentrations for ^{210}Po measured in El Hierro island were considerably higher both in volcano zone and in Las Canteras beach. The calculated CF in algae from both islands do not seem to show any noticeable difference. For the ratios among the radionuclides, those close to equilibrium were associated to conservative radionuclides (^{234}U , ^{238}U) and those in not equilibrium to reactive particle (^{234}Th , ^{210}Po and ^{210}Pb). Finally, two-way ANOVAs tested for differences in the radionuclides' activity concentrations and the activity concentration ratios, between the two areas (affected and non-affected) and sites within each area were performed. Significant differences between El Hierro and Las Canteras, mainly for ^{40}K and ^{234}Th were found.

1. Introduction

Radioactivity is a spontaneous phenomenon that occurs in the nucleus of unstable atoms, called radioactive nuclides or radionuclides, which transform/disintegrate into another stable or unstable isotope. This is due to an imbalance between the internal forces of the atom: while the electric force is responsible for the repulsion between the protons in the nucleus, the strong nuclear force is responsible for holding the protons and neutrons together. These processes involve the emission of particles and/or a large amount of energy in the form of ionizing radiation. The definitions of basic concepts in this first section can be found in any radioactivity book such as the one by Knoll (2000).

There are four types of radioactive decays which interact differently with matter and release different particles:

- **α decay:** an alpha particle or helium nucleus (${}^4_2\alpha = {}^4_2He$) is emitted as follows: ${}^A_ZX \rightarrow {}^{A-4}_{Z-2}Y + {}^4_2\alpha$. It involves high atomic masses and high particle speed, and it has the least penetrating power.
- **β^- decay:** an electron is emitted at high speed as follows: ${}^A_ZX \rightarrow {}^A_{Z+1}Y + \beta^- + \bar{\nu}_e$. This disintegration is typical of nucleus with large N/Z. β^- particles are more penetrating than alpha particles.
- **β^+ decay:** a positron is emitted at very high speed as follows: ${}^A_ZX \rightarrow {}^A_{Z-1}Y + \beta^+ + \nu_e$. It is typical of nucleus with small N/Z. They are similar in scope to β^- .
- **Electron capture:** no particles are emitted, there is only X-ray emission. Its decay scheme is: ${}^A_ZX^* \rightarrow {}^A_ZX + \gamma$. It is the most penetrating disintegration; it can only be stopped by a thick block of lead or concrete.

The radioactive decay of a population of N_i radionuclides is a random process that follows an exponential decay: $N_i(t) = N_i(0)e^{-\lambda_i t}$ (1), where λ_i is the radioactive decay constant, which is characteristic of each nuclide and decay process and is independent of the physical conditions. λ_i is related to the half-life period, T_i , the time in which the population is halved, as follows: $\lambda_i = \frac{\ln(2)}{T_i}$ (2).

Another concept that must be introduced is the specific activity or activity concentration, which is the activity per unit mass (Bq/Kg) or volume (Bq/L). The activity is the number of disintegrations per unit time and it is expressed in Becquerels (Bq) as: $A_i(t) = A_i(0)e^{-\lambda_i t}$ (3), where 1 Bq is 1 disintegration per second.

Ionizing radiation detection is based on its interaction with matter. The energy is deposited in the materials, mainly through the ionization and excitation of their atoms, but also, there can be light emission, temperature change or chemical effects. All this can

be an indicator of the presence of radiation. This radiation can be measured with different types of detectors: ionization chambers, such as Proportional Counters and Geiger-Mueller tubes, which are based on the effects produced by charged particles passing through a gas; scintillation detectors which detect ionizing radiation by the scintillation light produced in certain materials, and semiconductor detectors which are based on the property of semiconductor materials to vary their conductivity when receiving radiation, among others (Knoll, 2000). The two used in this work are semiconductor detectors: an Hyperpure Germanium gamma spectrometer and a Passivated Implanted Planar Silicon (PIPS) detector alpha spectrometer (see section 2.2. Gamma and Alpha spectrometry).

1.1 Radioactivity in the marine environment

The marine environment, like the entire natural environment, is inherently radioactive. Oceans cover approximately an area of $3.6 \cdot 10^8 \text{ km}^2$ and represent a huge reservoir of natural radioactivity. Natural radioactivity can be divided among two groups: the primordial radionuclides, which are those that have been in the Earth's crust since its formation; some of these may give rise to radioactive series, such as the series of ^{232}Th , ^{238}U and ^{235}U ; and the cosmogenic radionuclides that are produced by the interaction of cosmic rays with nucleus of the upper atmosphere (above 15 Km) (Livingston, 2005).

In oceanic water, some of the most abundant primordial radionuclides are: ^{40}K (45 $\mu\text{g/L}$), ^{87}Rb (34 $\mu\text{g/L}$), U (3.3 $\mu\text{g/L}$) and ^{232}Th (0.2 $\mu\text{g/L}$); the oceanic waters are impoverished in Thorium with respect to the continents due to the great stability of thorium minerals against those of uranium (Garzón Ruiperez, 1979). ^{210}Po and ^{210}Pb provide the major dose to marine organisms, being, therefore, the ones that contribute the most to the annual ingested radiation for those individuals who consume large amounts of fish and shellfish (Belivermiş et al., 2019). On the other hand, the most abundant cosmogenic radionuclides in ocean water are tritium, H_3 ($3.2 \cdot 10^{-12} \mu\text{g/L}$) and ^{14}C , in the form of CO_2 and carbonates ($3.1 \cdot 10^{-8} \mu\text{g/L}$) (Garzón Ruiperez, 1979).

Moreover, significant quantities of anthropogenic radionuclides have been released into the environment as a result of atmospheric weapon testing, nuclear weapon production activities and nuclear power fuel-cycle operations, in addition to accidents involving nuclear materials, intentional disposals, unexploded bomb accidents, waste dumping, nuclear-powdered submarines, satellite accidents and the general use of radioactive materials in medicine, industry, research and space exploration (Aarkrog, 2003; UNSCEAR, 2000). The main artificial radionuclides present in the ocean are fission products such as ^{90}Sr and ^{137}Cs , as well as transuranium elements originating from globally dispersed debris, and local and regional deposits from atmospheric nuclear weapons test, such as $^{239+240}\text{Pu}$, ^{99}Tc and ^{129}I (Livingston 2005; Kim et al., 2019).

Radionuclides, both natural and artificial, are taken up by marine organisms from water through adsorption/absorption, from food by the ingestion of prey organisms with already uptaken radionuclides and from sediments (Baltas, Kiris, & Sirin, 2017), by the ingestion of sediments with radionuclides or through the adsorption/absorption of the soluble radionuclides present in pore water between the sediment grains (Livingston, 2005; Fowler, 2011).

It has been shown that macroalgae can accumulate heavy metals from the water column, which may damage their tissues and inhibit certain functions (Praveen, Feroz, and Godwin, 2017; Uddin et al., 2019). Therefore, macroalgae are considered a good bioindicator for metal pollution in seawater, because of their high Concentration Factor (CF), which is defined as the ratio of the amount of radionuclide per unit fresh weight of tissue to that dissolved in an equal weight of seawater. Radionuclides are bioaccumulated and biomagnified along the marine food chain, altering the concentration of radionuclides in each trophic level. Bioaccumulation of radionuclides from seawater is also affected by environmental factors, such as temperature and salinity; radionuclide uptake rates correlate positively with temperature and show an inverse correlation with salinity. Recently, algae are more often in our diet; for this reason, the study of this community is of great importance (Chakraborty et al., 2014; Livingston, 2005).

1.2 Use of radionuclides as tracers of marine environmental processes

Radionuclides can be used as tracers for different environmental processes by measuring the activities of a parent nuclide and a daughter nuclide, from the same radioactive chain, which under normal conditions should be found in the medium in secular equilibrium ($A_{\text{parent}}(t) = A_{\text{daughter}}(t)$) but, due to a certain environmental process, the concentration of the daughter nuclide is increased or decreased. In this way, the daughter nuclide acts as a tracer for the process.

The radiotracer chosen must have a half-life close to the speed of the process. For example, ^{222}Rn is used to trace the ocean-atmosphere gas exchange (Cockenpot et al., 2015), ^{234}Th to measure the scavenging rates of the particles in the water column (Buesseler et al., 2009), ^{230}Th for the accumulative rates of sediments in the deep ocean (Lerner et al., 2018) and ^{226}Ra to trace ocean circulation (Burnett et al., 2008). For the determination of underwater discharges and volcanic processes (underground hydrogeology tracers), the descendants of the U/Th series, ^{222}Rn and the radioisotopes of Ra are used as tracers (Alonso et al., 2015).

^{222}Rn and ^{220}Rn in ground and surface waters have been used to predict earthquakes and volcanic eruptions, because it was suggested that radon ascended towards the upper part of the earth's crust through cracks or faults (Padilla et al., 2013). Consequently, soil

gas radon has been used in numerous occasions to understand and monitor submarine eruptive activity, like the volcanic events occurred in 2011-2012 at El Hierro Island in the Canary Archipelago, Spain (Padilla et al., 2013).

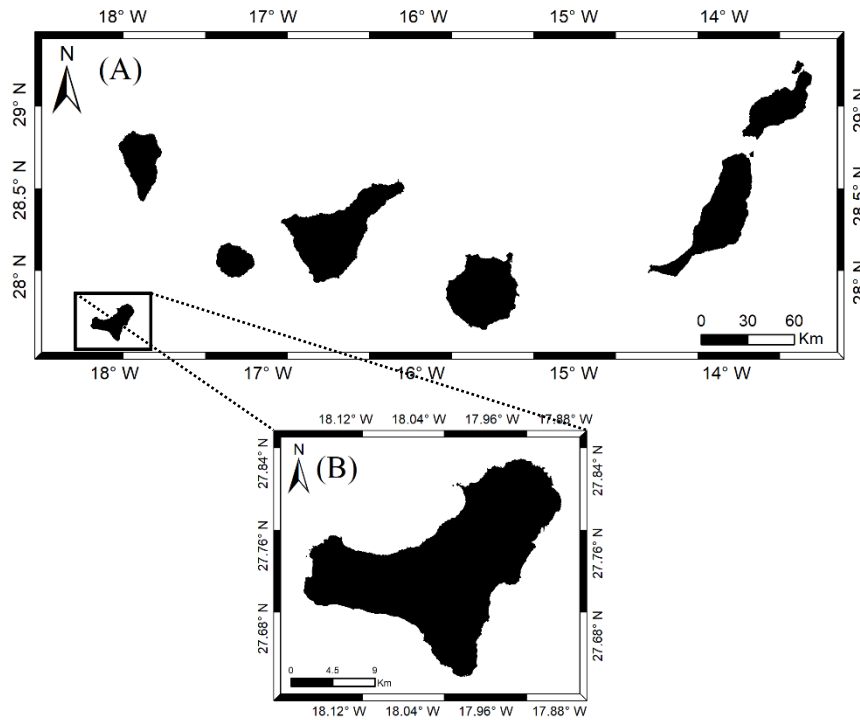


Figure 1. Location of the study area. (A) Canary Archipelago and (B) El Hierro island.

The Canary Islands (Fig. 1) are emerged on the continental shelf off the northwest African continental margin and they are thought to be the outcome of a mantle plume. This is supported by the theory of the westward decrease in the age of the islands, which ranges from 20.7 Ma for the oldest rocks in the easternmost island (Lanzarote) to only 1.12 Ma in the westernmost island of El Hierro (Urgeles et al., 1997). El Hierro is the westernmost volcanic edifice of the Canary Archipelago (Fig. 1) and the youngest island, which rises 5.5 Km above the 4000 m deep surrounding ocean floor. The island has a triangular shape with three well-defined major embayments: El Golfo, Las Playas and El Julán (Urgeles et al., 1997). As it is the youngest of the islands and it is supposed to be located directly above the location of the Canary Island hot spot, seismic and volcanic activity are expected to occur (Carracedo et al., 2012).

At the end of July 2011, in El Hierro, after more than two hundred years of repose, a large number of small earthquakes ($M < 2.5$) were registered at the north part of the island, between 8 and 15 Km inland, that lasted almost for 3 months. Then, the discrete earthquakes changed to a continuous tremor until an underwater eruption took place on October 12, 2011, located 2 Km south off La Restinga (the southernmost point of the island); the activity lasted until March 2012 (Padilla et al., 2013).

During the submarine eruption it was observed a large water discoloration area due to the intense discharge of high temperature hydrothermal fluids, magmatic gases and steamy lava fragments. Soil gas radon and soil gas CO₂ increased during the seismic activity, as a result of rock fracturing (Padilla et al., 2013). Moreover, due to the volcanic discharges, abrupt changes in the physical-chemical properties of seawater took place. As explained by Santana-Casiano et al., (2013) the carbonate system was modified, and the pH reduced as a consequence of the emission of magmatic gas and other compounds, leading to a severe acidification. The redox potential and the amount of dissolved oxygen were reduced due to the emission of reduced species and Fe (II). A natural fertilization occurred, as different nutrients (Fe, Si, P and N) were released into the seawater. Consequently, although the volcano was responsible for eradicating most of the marine life, it also contributed to its own regeneration by increasing the productivity in the area. In an earlier study (Betancor et al., 2014), the effects of the submarine eruption on the morphology, photosynthesis and physiological performance of two of the most abundant brown algae, *L. variegata* and *Padina pavonica* were studied, showing a higher impact on the calcareous seaweeds, *P. pavonica*, than on the non-calcareous seaweeds, *L. variegata*.

Apart from using radionuclides as tracers of different volcanic processes, it is important to be able to characterize the radiological impact produced by the emission of radionuclides in an underwater volcanic eruption, both to the environment, the marine organisms, and eventually to the surrounding population.

The objective of this project is to characterize the radiological impact in the surroundings of the Tagoro submarine volcano, several years after its eruption. A previous study on the radiological impact of the Tagoro volcano on costal sediment samples (Obispo and Escobar, 2019) showed higher values of ²²⁶Ra in the southwest of El Hierro, assigning this increase to the *Restingolites* released during the underwater eruption. Following the same line of research, in this study, samples of the brown algae *Lobophora variegata* (Fig. 2) were collected along the coastal perimeter of El Hierro Island, with the aim of using them as an environmental dosimeter due to their high accumulation power to test if we could find a same impact.

A previous study by Tejera et al. (2019) showed that the specie *L. variegata* achieved maximum mean activity concentrations for ²¹⁰Po and ²¹⁰Pb. Additionally, the choice of this algae is motivated by its high large abundances around the entire island; it is commonly found on rocky substrates in the intertidal zone up to a depth of 30 m (Tuya and Haroun, 2006; Espino et al., 2007).

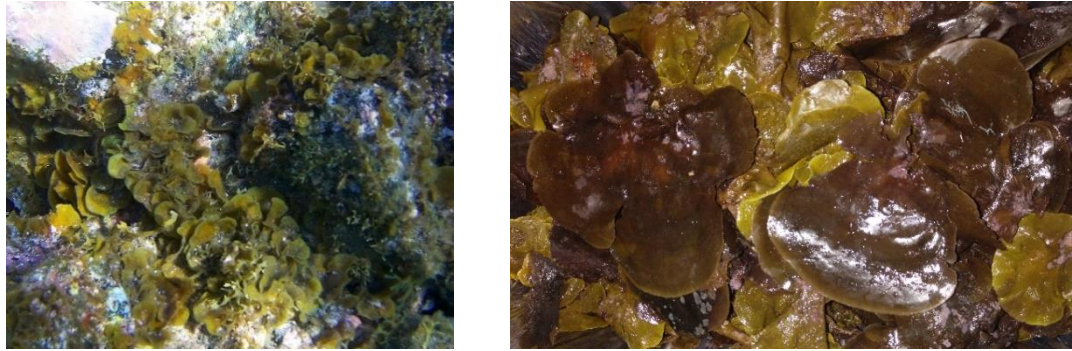


Figure 2. Samples of the algae *Lobophora variegata* (own photos).

The activity concentrations of the samples from El Hierro were compared with those of samples collected in Las Canteras beach, Las Palmas de Gran Canaria, thus acting as reference not influenced by the volcanic eruption; furthermore, the results were also compared with previous studies of the region also carried out with algae samples.

2. Materials and methods

2.1. Sampling and sample preparation

Samples of the algae *L. variegata* were collected in the intertidal along the coast of El Hierro island in a first campaign in February 2020 and in a second in August 2020. Because of the characteristics of the different locations, some samples had to be collected at high tide, while others were collected preferentially at low tide; in this way, the depth of the samples ranged from 1 m to 4 m deep. Whenever possible, two samples, separated approximately 50 m apart, were collected at the same location. In addition, water samples were also collected and stored in 2 L polyethylene containers. The location of the sampling sites is shown in Figure 3 and the code for the sites in Table 1.

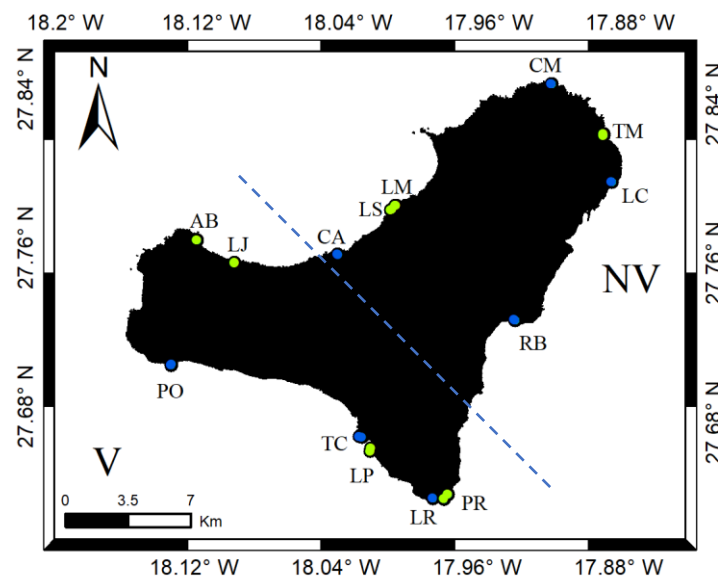


Figure 3. Sampling points along the coast of El Hierro island. Blue dots indicate that both algae and seawater were sampled. Green dots indicate that only algae were sampled.

The distribution of the sampling points was chosen to obtain a representative number of samples around the entire island perimeter. This strategy allowed us to track the radiological impact on the algae, resulting from the radionuclide emissions from the Tagoro underwater volcano. Therefore, the island was divided into two different zones: one area affected by the submarine eruption (V), and another one considered unaffected (NV) (see Fig. 3). This division was done according to the satellite images analysed by Eugenio et al. (2014), in order to monitor the environmental impact caused by the underwater volcanic eruption.

The different sites where the algae were collected, the code for each sample and the campaign's day are displayed in Table 1. Notice that samples of *L. variegata* were also gathered from Las Canteras beach, in Las Palmas de Gran Canaria, to be used as reference samples not influenced by the volcanic eruption of El Hierro.

Table 1. Code, sites and date of campaign for the samples from El Hierro island and Gran Canaria.

Code	Site	Date	Code	Site	Date
CM*	Charco Manso	06/02/2020	LP*	Las Lapillas	15/08/2020
LC	La Caleta	06/02/2020	PR*	Punta del Río	20/08/2020
RB*	Roque de la Bonanza	06/02/2020	LM*	Las Macetas	31/08/2020
LR	La Restinga	07/02/2020	LS*	Los Sargos	31/08/2020
TC*	Tacorón	07/02/2020	LJ*	La Laja	31/08/2020
PO*	Punta de Orchilla	08/02/2020	CA*	Charco Azul	01/09/2020
TM*	Tamaduste	02/08/2020	AB	Arenas Blancas	01/09/2020
Code	Site	Date			
APLC19*	Las Canteras, LPGC	11/12/2019			
APLC20_1	Las Canteras, LPGC	30/04/2020			
APLC20_2	Las Canteras, LPGC	19/06/2020			

(*) Two samples separated 50 m were collected.

To prevent the growth state of the algae from interfering with the results, only those algae that were in an adult state were chosen. Adult thallus were collected at all times and locations. Once collected, they were washed *in situ* with seawater to remove remains of sediments, other algae, or marine organisms. They were stored in insulating bags and kept in a cold container.

Samples were taken to the laboratory where they were dried in an oven at 80 °C for 24 h. They were weighted before and after drying to further calculate the relation between Dry and Fresh Weight (DW/FW). Algae were crushed with an electric mixer and filtered through a 1 mm mesh size sieve. Finally, samples were saved in PVC trunk-conical containers and sealed with aluminium strips which acted as a barrier to radon and prevented it from leaking. The samples in the bottles had to reach a height of 2.5 cm for

its correct measurement in the gamma detector (Fig. 4). An aliquot of 0.5 g of each sample was separated to be analysed through alpha spectrometry.

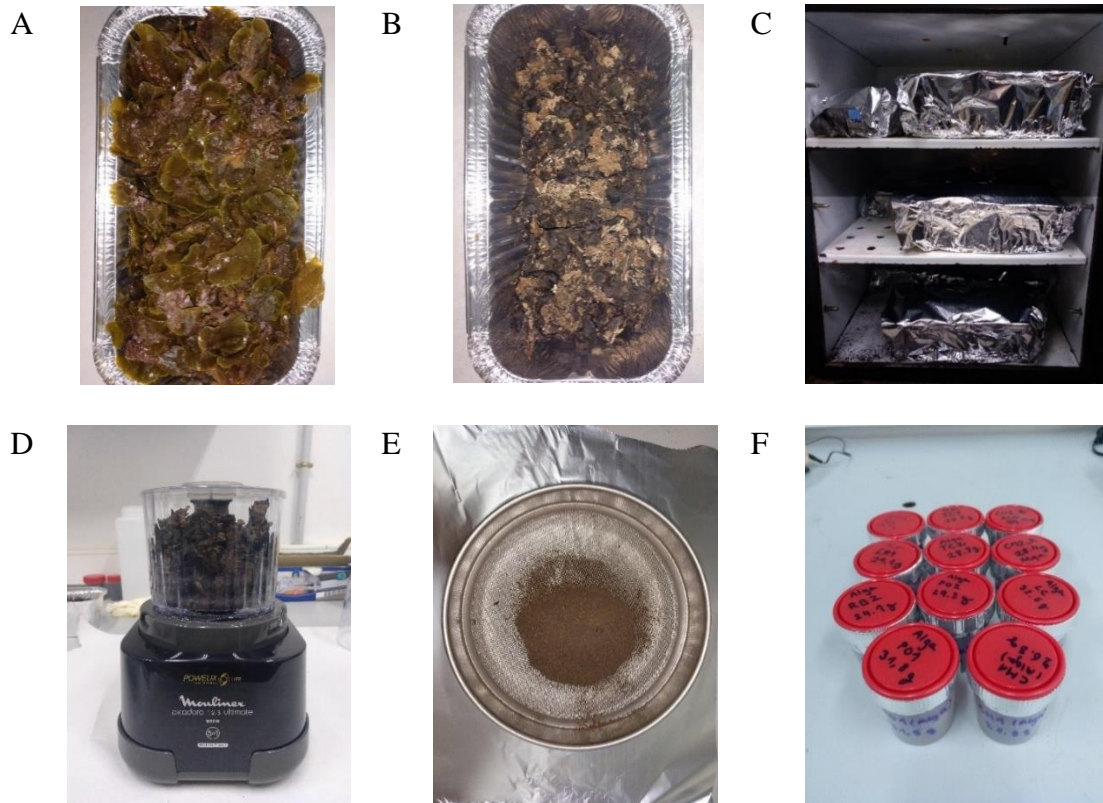


Figure 4. Fresh (A) and dried (B) samples deposited in aluminium trays; (C) samples placed inside the oven; (D) sample grinding with the mincer; (E) sample filtering through a 1 mm mesh size sieve, and (F) PVC trunk-conical containers sealed with aluminium strips containing all samples.

Regarding the water samples, once in the laboratory they were filtered with a vacuum filtration assembly to remove solid debris and were acidified to avoid the proliferation of biological life and thus be preserved. Afterwards, they were stored in polyethylene container until their measurement with alpha and gamma spectrometry.

2.2. Gamma and alpha spectrometry

2.2.1. Gamma spectrometry technique

Gamma spectrometry measurements were made with a Canberra Extended Range (XtRa) coaxial Germanium spectrometer, model GX3518. It has a carbon composite window (0.6 mm thick), 153 cm³ of active volume and 5 mm length from the detector to the carbon window. Its relative efficiency is 35% and nominal FWHM of 0.875 keV at 122 keV and 1.80 keV at 1.3 MeV. It works coupled to a DSA-1000 Canberra multichannel analyser and is shielded with 15 cm thick iron and located in a room with walls and ceiling made of concrete in the ground floor of a three-floor building, to minimize background radiation. The spectral analysis was carried out using the Canberra Genie 2000 software package (Arnedo et al., 2017, 2013).

For the algae samples, stored in the PVC trunk-conical containers, two measurements were made: a first measurement was carried out within the first week after sample collection, to guarantee the equilibrium between ^{224}Ra and ^{212}Pb and to be able to detect short-lived isotopes, and a second measurement, after one month, to ensure the secular equilibrium between ^{226}Ra and ^{214}Pb . The radionuclides whose activity concentrations were determined from the ^{238}U series (decay series in Annex I.I) were: ^{234}Th , measured through the average of the activities of two of its photopeaks, 63.29 keV and 93.56 keV (1st meas.); ^{226}Ra determined from the 2nd meas. of ^{214}Pb emission peak of 351.92 keV; ^{210}Pb identified by its emission line of 46 keV (2nd meas.), and ^{234}Pa . (1001 keV), not actually used as it was already in equilibrium with ^{234}Th . From the ^{232}Th series (Annex I.II) the radionuclides were: ^{224}Ra from the first measurement of ^{212}Pb (emission line of 238.63 keV) and ^{228}Th from the equilibrium measurement of ^{212}Pb . It was also detected ^{40}K (1460.81 keV), whose activity was obtained as an average value between both measurements since it is a long-lived isotope. ^7Be (477.6 keV), ^{137}Cs (661.65 keV), ^{208}Tl (583.19 keV), ^{214}Bi (609.31 keV) and ^{228}Ac (911.6 keV) were also detected in some of the samples, but their values were always found below the MDA (Minimum Detectable Activity), so they have not been included in the results. The measures lasted one day.

As for the water samples, they were placed inside the gamma detector stored into Marinelli vessels. Only one measurement was carried out in the conditions of secular equilibrium, a month after its collection. Although some of the radionuclides mentioned above were detected in some of the samples, they were always found below the MDA; only the activity concentration of ^{40}K was measured above the MDA in all samples. Due to lower radionuclides' activity in seawater, their measures lasted between 2-3 days.

2.2.2. Alpha spectrometry technique

The detection system used was the Alpha Analyst A450-18AM model from the Canberra brand, with an active area of 450 mm² and a resolution of 18 keV. It consists of 12 individual spectrometric units, each one equipped with a PIPS detector located inside a vacuum chamber. The analogic signal is converted into a digital signal by the ADC (Analog to Digital Converter) and a spectrum is generated from the distribution of the number of pulses in the different channels by the MCA (Multi Channel Analyser). The Alpha Analyst software package with the Genie 2000 applet was used for the acquisition and analysis of spectra (Canberra, 2017).

Alpha spectrometry technique allowed the determination of uranium isotopes (^{234}U , ^{235}U and ^{238}U), thorium isotopes (^{232}Th , ^{230}Th and ^{228}Th) and ^{210}Po . To determine the activity concentrations of the different radioisotopes, the radionuclides were separated and purified by a radiochemical treatment. In order to measure the yield and therefore, to

know the original quantity of radioisotopes in the samples, a known quantity of an artificial tracer was added to the samples. It was assumed that the tracer was affected in the same way as the isotopes we wanted to measure, so knowing the initial and final amount of the added tracer, we were able to calculate the losses that our procedure entailed. The tracers used were: ^{232}U ($A = 75.79 \pm 1.60 \text{ Bq/Kg}$), ^{229}Th ($A = 76.3 \pm 1.2 \text{ Bq/Kg}$) and ^{209}Po ($A = 71.51 \pm 1.25 \text{ Bq/Kg}$).

Pretreatment and conditioning differs between liquid and solid samples.

- **Liquid samples:** seawater samples were poured into a beaker along with 0.5 mL of each tracer, and with the precipitators KMnO_4 and MnCl_2 ; it was left homogenizing for 2 h (Fig. 5A). The pH of the sample was then adjusted to around a value of 8 – 9 by adding ammonia (NH_3 at 30%). It was homogenized for 4 h and it was left to rest 8 h so that a precipitate which contained the radionuclides was formed (Fig. 5B). Finally, the filter precipitate was dissolved in a beaker with 20 – 30 mL of 1.2 M HCl and H_2O_2 at 6% solution and brought to dryness (Blasco et al., 2016; Oliveira and Carvalho, 2006).
- **Solid samples:** an aliquot of 0.5 g of each algae sample was weighted and spiked with ^{232}U , ^{229}Th and ^{209}Po as yield monitors. Then they were digested in savillex vessels using a combination of HF , HNO_3 and H_2O_2 in an oven for at least 72 h at 90 °C. The solution was then transferred to a teflon vessel and it was ready to start the adaptation to nitric and the separation and extraction of the different radionuclides (Hierro et al., 2012; Oliveira and Carvalho, 2006).

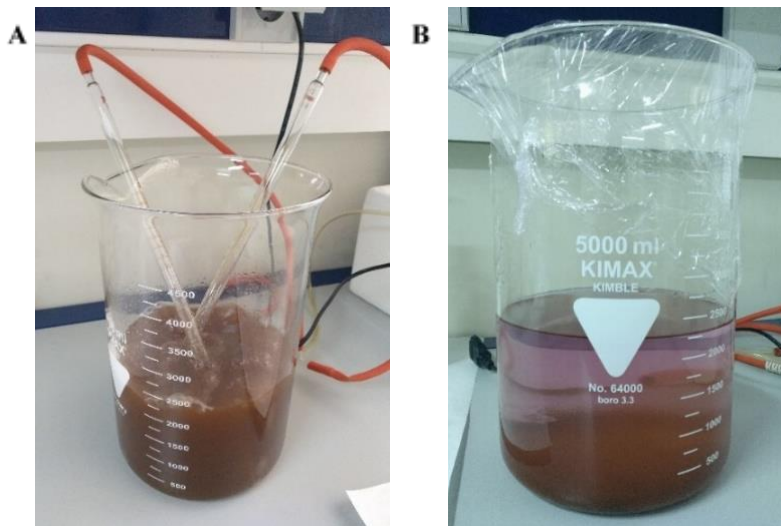


Figure 5. Water sample being homogenized (A) and the precipitate formed after homogenization (B) (own photos).

The procedure described hereafter is common for both liquid and solid samples. We added 5 mL of 37% HCl solution and we brought to dryness, always below 80 °C to avoid polonium volatilization; this step was performed twice. Then we repeated twice the process of adding 10 mL of 69% HNO₃ and bringing the solution to dryness. Finally, another 5 mL of 8 M HNO₃ were added and brought to dryness.

Isolation and autodeposition of Polonium

It then followed the sequential extraction method based on trybutylphosphate (TBP) to separate the ²¹⁰Po from the actinides (Oliveira & Carvalho, 2006). The initial solution was poured into a separatory funnel with nitric acid and TBP. After a stirring and decanting process, the isotopes of the actinides that had formed complex compounds linked to the chains of the organic solvent were collected in a vessel; Po and other isotopes remained in the original aqueous phase. To the solution containing the Po it was added hydrochloric acid and ascorbic acid. It was poured into a bottle with a silver disc, and it was left automatically stirring overnight, allowing the spontaneous deposition of the polonium. The silver disk was then ready to be measured by the alpha spectrometer (Mouloud Lehitani, 2012; Oliveira & Carvalho, 2006).

Extraction and purification of Thorium and Uranium

To isolate the actinides, a sequential well-established radiochemical method based on extraction chromatography was applied (Hierro et al., 2012). For the extraction of Th from the phase that remained after the Po extraction we proceeded in the same way. In this case, the solvent used was xylene and hydrochloric acid. After stirring and settling, Th was in the aqueous phase that was extracted, while U remained in the organic phase. However, thorium's solution could contain traces of uranium, so it was purified by passing the sample through an ion exchange resin that retained any U isotopes. The column had to be preconditioned several times with 8M HNO₃ and Th was finally extracted with 40 mL of 9 M HCl. Th was then sufficiently purified to be electroplated. Uranium isotopes were extracted from the remaining organic phase by adding distilled water to the separatory funnel (Oliveira & Carvalho, 2006).

Electrodeposition of Uranium and Thorium

The process consisted of fixing the actinides on a steel disk by electrolysis. H₂SO₄ was added to both solutions and thymol blue as a pH indicator; with NH₃ we adjusted the pH between 2.2 and 2.5. The disks were placed inside the electrodeposition cells and the solutions were poured into them. It then followed the electrodeposition by placing the cell 4 – 5 mm from the electrode, at 1.2 A for 1 h in the case of uranium and at 1.5 A for 2 h in the case of thorium (Mouloud Lehitani, 2012).

2.3. Activity concentrations

The specific activity (Bq/Kg) of the isotopes was estimated with the following expression (Arnedo, 2014):

$$A_{el} = \frac{N_I}{\varepsilon t I r m} \quad (4)$$

where N_I is the net number of counts of the isotope peak, ε is the detector efficiency (%), I is the intensity of the radioactive emission detected, r is the measurement yield, t is the counting time (s), and m is the sample mass (g).

The uncertainty associated to this activity was expressed as (Arnedo, 2014):

$$u(A_{el}) = A_{el} \sqrt{\frac{1}{N_I} + \frac{1}{N_t}} \quad (5)$$

2.4. Data analysis

2.4.1. Activity corrections

^{210}Po specific activity measured through α -spectrometry had to be corrected on the deposition date, the moment at which there is only ^{210}Po decay since there is no longer production of polonium by ^{210}Pb (decay series in Annex I.D); and it was then corrected to the date of collection, when the algae stopped absorbing radionuclides from seawater.

These corrections were carried out using the Bateman equations which, in a simplified way, would be as follows (Cetnar, 2006):

- When there was only radioactive decay of a parent nuclide into a daughter nuclide, we used Eq. (1), $A_B(t) = A_B(0)e^{-\lambda_B t}$, where time t would be the moment of measurement and $t = 0$ the moment of deposition.
- If the daughter nuclide was also radioactive, thus forming a radioactive chain or series, in which the radionuclide of interest was being produced and disintegrated at the same time, we used:

$$A_B(t) = A_B(0)e^{-\lambda_B t} + A_A(0) \frac{\lambda_B}{\lambda_B - \lambda_A} (e^{-\lambda_A t} - e^{-\lambda_B t}) \quad (6)$$

Which corresponds to the decay series: $A \xrightarrow{\lambda_A} B \xrightarrow{\lambda_B} C(\text{stable})$. In this case, A would correspond to ^{210}Pb , obtained from the second measurement by γ -spectrometry, and B to ^{210}Po ; time t would be the moment of deposition and $t = 0$ the moment of sampling collection.

The specific activity of ^{234}Th measured through γ -spectrometry had to be corrected on the date of campaign as mentioned above.

2.4.2. Statistical analysis

Two-way ANOVAs tested for differences in the radionuclides' activity concentrations and the activity concentration ratios, between the two areas (adjacent vs. far away from the underwater volcano) and sites within each area. "Area" was considered a fixed factor, while "sites" was a random factor nested within each area. Data was square-root or log (x+1) transformed to meet parametric assumptions (normality of residuals and homogeneous variances). All analyses were performed using the R statistical package. The R-package ggplot2 was used to graphically visualize data via boxplots.

Statistically significant differences are considered to be those with p-value is below 0.05; however, for those activity concentrations or ratios between radionuclides whose p-values were below 0.20 and that with the corresponding boxplots certain differences could be observed, we have also considered them to be relatively different.

2.5. Performance criteria

Finally, in order to validate the methodology used and to ensure the quality of our results, we measured by both the alpha and gamma spectrometry an IAEA Certified Reference Material similar to the samples measured, the IAEA-446, which corresponds to a brown algae from the Baltic Sea (*Fucus vesiculosus*) (Pham et al., 2014).

The accuracy and precision were calculated by the standard tests used commonly in proficiency tests by the IAEA. Such tests were:

- U_{test} or U-score, used to determine if the results differ significantly from the expected value at a given level of probability, calculated as (IAEA, 2010):

$$U_{test} = \frac{|Value_{IAEA} - Value_{Analyst}|}{\sqrt{Unc_{IAEA}^2 + Unc_{Analyst}^2}} \quad (7)$$

- Precision Score (P-score) calculated as (IAEA, 2010):

$$P = \sqrt{\left(\frac{Unc_{IAEA}}{Value_{IAEA}}\right)^2 + \left(\frac{Unc_{Analyst}}{Value_{Analyst}}\right)^2} \times 100\% \quad (8)$$

Both tests involve the activity values and uncertainties of the radionuclides measured at the laboratory and those of reference from the IAEA. It has been considered acceptable a U_{test} value below 2.58 for a level of probability at 99% and a precision value below the Limit of Acceptable Precision ($P < LAP$); the LAP values are assigned based on the activity of each radionuclide: 15% for $A > 5$ Bq/Kg, 20% for activities between 1 and 5 Bq/Kg and 25% for $A < 1$ Bq/Kg (IAEA, 2010).

The results of both tests between the measured activities and those of the reference materials were below the accepted limits (u-test < 2.58 and p-score < 20%), thus proving the quality of both measurement techniques.

3. Results and discussions

3.1. Radionuclides activity concentrations

This first analytical description is based on the samples collected from El Hierro in the campaign in February and those collected in Las Canteras beach, Gran Canaria.

Table 2 contains the different activity concentrations of the natural radionuclides present in the samples by the alpha spectrometry: ^{234}U , ^{235}U , ^{238}U and ^{210}Po . Regarding the activity concentrations of the thorium isotopes mentioned in the methodology, their energy spectra had to be discarded because there was too much peak overlap to allow us a proper identification of the radioisotopes.

Table 2. Activity concentrations and their means (Bq/Kg) of the alpha emission radionuclides for *L. variegata* samples from El Hierro and Las Canteras (Gran Canaria). DW/FW is the ratio between dry and fresh weight.

Sample	DW/FW	^{234}U	^{235}U	^{238}U	^{210}Po
CM1	0.205	5.7 ± 0.4	0.15 ± 0.06	4.7 ± 0.4	336 ± 17
CM2A	0.179	6.9 ± 0.6	0.18 ± 0.08	6.2 ± 0.6	347 ± 16
CM2B	0.166	8.6 ± 0.9	0.12 ± 0.08	6.7 ± 0.7	269 ± 15
LC	0.218	9.2 ± 0.6	0.28 ± 0.08	6.9 ± 0.5	308 ± 13
LR1	0.206	4.4 ± 0.5	0.42 ± 0.14	4.7 ± 0.5	204 ± 13
PO1	0.211	6.3 ± 0.5	0.27 ± 0.08	4.6 ± 0.4	259 ± 11
PO2	0.173	7.9 ± 0.6	0.28 ± 0.11	6.4 ± 0.6	276 ± 11
RB1	0.209	7.7 ± 0.7	0.08 ± 0.06	5.8 ± 0.6	235 ± 22
RB2	0.221	7.2 ± 0.5	0.23 ± 0.08	5.3 ± 0.4	291 ± 13
TC1	0.164	6.7 ± 0.7	0.06 ± 0.06	6.5 ± 0.7	206 ± 10
TC2	0.201	6.2 ± 0.6	0.09 ± 0.06	3.9 ± 0.5	233 ± 11
Mean	0.196	7.0 ± 0.6	0.20 ± 0.08	5.6 ± 0.5	270 ± 14
APLC19_1	0.253	10.0 ± 0.8	0.32 ± 0.11	9.9 ± 0.8	228 ± 19
APLC19_2	0.242	10.1 ± 0.8	0.24 ± 0.09	10.1 ± 0.8	319 ± 15
APLC20_1	-	7.5 ± 0.7	0.43 ± 0.14	7.2 ± 0.6	243 ± 11
APLC20_2	0.231	7.9 ± 0.7	0.12 ± 0.07	7.0 ± 0.7	306 ± 16
Mean	0.242	8.9 ± 0.7	0.27 ± 0.10	8.5 ± 0.7	274 ± 15

In Table 3 we present the values of the activity concentrations measured by the gamma spectrometer for the following radionuclides: ^{234}Th , ^{226}Ra , ^{210}Pb , ^{228}Th and ^{40}K . Activity concentrations obtained for ^{224}Ra were practically in secular equilibrium with those of obtained for ^{228}Th .

Table 3. Activity concentrations and their means (Bq/Kg) of the gamma emission radionuclides for *L. variegata* samples from El Hierro and Las Canteras (Gran Canaria).

Sample	²³⁴ Th	²²⁶ Ra	²¹⁰ Pb	²²⁸ Th	⁴⁰ K
CM1	1420 ± 60	4.0 ± 1.6	92 ± 8	4.9 ± 1.3	1090 ± 50
CM2A	1680 ± 70	7.6 ± 1.7	107 ± 7	6.0 ± 1.2	1170 ± 50
CM2B	1570 ± 60	8.9 ± 1.4	97 ± 7	6.8 ± 1.0	1240 ± 60
LC	1470 ± 60	4.7 ± 1.3	101 ± 7	5.6 ± 1.1	980 ± 50
LR1	1160 ± 50	6.8 ± 1.5	55 ± 7	4.3 ± 1.1	1180 ± 60
PO1	1440 ± 60	5.8 ± 1.4	65 ± 7	4.9 ± 1.1	990 ± 50
PO2	1980 ± 80	6.5 ± 1.6	112 ± 9	8.4 ± 1.4	1190 ± 60
RB1	1890 ± 80	5.1 ± 1.5	141 ± 9	5.8 ± 1.2	1060 ± 50
RB2	1949 ± 80	5 ± 2	95 ± 9	7.3 ± 1.3	1180 ± 60
TC1	1390 ± 60	8.3 ± 1.1	94 ± 8	6.4 ± 1.2	1120 ± 50
TC2	1380 ± 60	8.3 ± 1.8	72 ± 8	5.5 ± 1.3	1030 ± 50
Mean	1570 ± 60	6.5 ± 1.5	94 ± 8	6.0 ± 1.2	1110 ± 50
APLC19_1	720 ± 30	5 ± 2	95 ± 10	4.9 ± 1.7	1330 ± 60
APLC19_2	630 ± 30	12.2 ± 1.4	71 ± 6	9.7 ± 1.0	1340 ± 60
APLC20_2	460 ± 20	8.6 ± 1.5	65 ± 7	6.5 ± 1.2	1200 ± 50
Mean	600 ± 30	8.6 ± 1.7	77 ± 8	7.0 ± 1.3	1290 ± 50

For the discussion of this section, we have considered different areas around El Hierro island according to the satellite images presented by Eugenio et al. (2014) which were used to monitor the submarine eruption and the temporal evolution of stain in the days after the eruption. In this way, the areas concerned and the sites included in each of them are: None Volcano area (NV) with Charco Manso, La Caleta, Roque de la Bonanza and Charco Azul; Restinga Zone (RZ) with La Restinga and Tacorón, and the Stain area (S) with Punta de Orchilla.

Comparing the means obtained for the different radionuclides' activity concentrations for samples in El Hierro (EH) and in Las Canteras (PLC), the most significant difference can be found with ²³⁴Th, which has a higher value in EH, (1570 ± 60) Bq/Kg, than in PLC, (600 ± 30) Bq/Kg. From the same decay series, the specific activity of ²³⁸U is slightly lower in EH, (6.1 ± 0.6) Bq/Kg, than in PLC, (8.5 ± 0.7) Bq/Kg, and the same occurs with ²³⁴U, for which a specific activity of (7.4 ± 0.6) Bq/Kg is measured in EH compared to (8.9 ± 0.7) Bq/Kg measured in PLC. Higher values for ²¹⁰Pb are found in EH than in PLC, being (94 ± 8) Bq/Kg and (77 ± 8) Bq/Kg respectively. On the other hand, in the PLC area we have obtained higher values of ⁴⁰K than in EH zone, being respectively (1290 ± 50) Bq/Kg and (1100 ± 50) Bq/Kg.

If we only take into account samples gathered in El Hierro in order to study differences between the area affected by the volcano and the one that was not directly influenced, we

find the following: the activity of ^{234}Th is slightly lower in the RZ than in the NV and S areas, being (1310 ± 50) Bq/Kg, (1660 ± 70) Bq/Kg and (1710 ± 70) Bq/Kg respectively. The same occurs with ^{234}U for which the specific activities are (5.8 ± 0.6) Bq/Kg in RZ, (7.5 ± 0.6) Bq/Kg in NV and (7.1 ± 0.6) Bq/Kg in S area. Regarding ^{210}Pb we have also found some differences: its activity concentration in the S and RZ areas, the ones affected by the submarine volcano, is lower than that of the NV area, being (89 ± 8) Bq/Kg, (74 ± 8) Bq/Kg and (102 ± 8) Bq/Kg respectively.

As for the water samples, ^{40}K was the only radionuclide measured through gamma spectrometry whose activity was above the detection limit. The activity concentration values for ^{234}U , ^{235}U , ^{238}U and ^{210}Po , detected through alpha spectrometry, were also calculated. Because of a low number of water samples were collected, we have only distinguished between non-volcano area, NV, and the volcano area, V (i.e. La Restinga and Stain zones), where it has been included the water sampled in Punta de Orchilla. The mean value for Las Canteras beach was obtained by averaging the activity concentrations measured in four samples collected in December 2019 and April 2020.

Table 4. Activity concentrations and their means (Bq/L) for the radionuclides in water samples from El Hierro and Las Canteras, Gran Canaria. Activity concentration values for radionuclides in coastal marine waters from Hosseini et al. (2010) have also been included as reference values.

Nuclide	El Hierro			Las Canteras	Coastal waters
	V	NV	EH Mean	PLC Mean	
^{40}K	15.3 ± 1.0	14.5 ± 0.9	14.8 ± 1.0	13.8 ± 0.8	12
^{234}U	0.047 ± 0.003	0.042 ± 0.002	0.045 ± 0.003	0.042 ± 0.003	0.047
^{235}U	0.0015 ± 0.0004	0.0010 ± 0.0002	0.0013 ± 0.0003	0.0013 ± 0.0003	0.0019
^{238}U	0.040 ± 0.003	0.037 ± 0.002	0.039 ± 0.002	0.037 ± 0.003	0.041
^{210}Po	0.0052 ± 0.0003	0.0045 ± 0.0003	0.0054 ± 0.0004	0.0026 ± 0.0003	0.002
^{234}Th	BLD	BLD	BLD	BLD	0.012
^{226}Ra	BLD	BLD	BLD	BLD	0.0034
^{210}Pb	BLD	BLD	BLD	BLD	0.047
^{228}Th	BLD	BLD	BLD	BLD	0.0003

*BLD: below detection limit (<MDA)

No differences can be noticed within the radionuclides measured in both islands except for the ^{210}Po , whose value is slightly higher in the V area than in the NV area, implying a higher mean value of the activity concentration in EH than in PLC, which are (0.0054 ± 0.0004) Bq/Kg and (0.0026 ± 0.0003) Bq/Kg respectively.

Likewise, all values are in good harmony with those found in coastal waters, except for the value of ^{210}Po measured in El Hierro island which is considerably higher.

A possible hypothesis of ^{210}Po increment could be the enrichment of the water by ^{238}U series radionuclides due to eruptions and degasses processes of Tagoro volcano. One of this could be ^{226}Ra which is a radioisotope with a half-life of 1600 years, and if, as it was seen in the sediments samples from El Hierro by (Manzanares et al., 2019), it increased its concentration due to the emissions of Restingolites with the volcanic eruption, it would be explained this increase in ^{210}Po in the affected areas, as ^{226}Ra would have been acting as a source for polonium since then. However, ^{226}Ra could not be measured in water samples because its concentration in seawater is too low to be measured with the instruments available; for this reason, in this work we intended to use algae for its high accumulation power as a natural dosimeter of radioactivity in seawater.

In summary, in this section we have apparently found some differences between El Hierro and Gran Canaria islands and within the areas considered around El Hierro, some of which could be suitable with an impact of the volcano on the activity concentrations of radionuclides measured in the brown algae *L. variegata*. Lower values for ^{234}Th and ^{234}U have been measured in La Restinga zone than ones obtained in the other areas. ^{210}Pb was also lower in La Restinga zone and the stain area than in the unaffected area. Moreover, the highest values of ^{234}Th and ^{210}Pb were found in El Hierro, while activity concentrations for ^{238}U , ^{234}U and ^{40}K were higher in Las Canteras.

3.2. Concentration factors

The concentration factor of *L. variegata* samples from the different sites was also calculated and the values are shown in Table 5. As previously defined in section 1.1. *Radioactivity in the marine environment*, the CF gives an idea of the accumulative power of the algae for each of the measured radionuclides present in its surrounding seawater.

For those radionuclides whose activities could be measured in seawater samples, the CFs have been calculated at each site using the mean activity concentrations in seawater according to the area to which it corresponded, either V, NV, or PLC. Only in the case of those radionuclides that could not be measured at the laboratory (^{234}Th , ^{226}Ra , ^{210}Pb and ^{228}Th) we used the reference value of Hosseini et al. (2010) to calculate the CFs.

Despite this, for those radionuclides that we could measure in seawater, we also calculated the CFs using the reference values of coastal marine waters and both results were in perfect harmony as one would have expected considering the few differences found in the activity concentrations measured in seawater samples displayed in Table 4.

As done in the previous section, calculating the means of the CFs in the areas of NV, RZ and S, what one finds is that apparently there are no significant differences.

Table 5. Concentration factors (L/Kg) of the different radionuclides for *L. variegata* samples collected at the different sites, and their means in El Hierro and Las Canteras.

Sample	²³⁴ U	²³⁵ U	²³⁸ U	²¹⁰ Po	²³⁴ Th	²²⁶ Ra	²¹⁰ Pb	²²⁸ Th	⁴⁰ K
CM1	3x10 ¹	3x10 ¹	3x10 ¹	2x10 ⁴	2x10 ⁴	2x10 ²	9x10 ³	3x10 ³	2x10 ¹
CM2A	3x10 ¹	3x10 ¹	3x10 ¹	1x10 ⁴	3x10 ⁴	4x10 ²	1x10 ⁴	4x10 ³	1x10 ¹
CM2B	3x10 ¹	2x10 ¹	3x10 ¹	1x10 ⁴	2x10 ⁴	4x10 ²	8x10 ³	4x10 ³	1x10 ¹
LC	5x10 ¹	6x10 ¹	4x10 ⁰	1x10 ⁴	3x10 ⁴	3x10 ²	1x10 ⁴	4x10 ³	1x10 ¹
LR1	2x10 ¹	6x10 ¹	2x10 ¹	8x10 ³	2x10 ⁴	4x10 ²	6x10 ³	3x10 ³	2x10 ¹
PO1	3x10 ¹	4x10 ¹	2x10 ¹	1x10 ⁴	3x10 ⁴	4x10 ²	7x10 ³	3x10 ³	1x10 ¹
PO2	3x10 ¹	3x10 ¹	3x10 ¹	9x10 ³	3x10 ⁴	3x10 ²	1x10 ⁴	5x10 ³	1x10 ¹
RB1	4x10 ¹	1x10 ¹	3x10 ¹	1x10 ⁴	3x10 ⁴	3x10 ²	1x10 ⁴	4x10 ³	2x10 ¹
RB2	4x10 ¹	3x10 ¹	3x10 ¹	1x10 ⁴	4x10 ⁴	3x10 ²	1x10 ⁴	5x10 ³	2x10 ¹
TC1	2x10 ¹	6x10 ⁰	3x10 ¹	7x10 ³	2x10 ⁴	4x10 ²	8x10 ³	4x10 ³	1x10 ¹
TC2	3x10 ¹	1x10 ¹	2x10 ¹	9x10 ³	2x10 ⁴	5x10 ²	7x10 ³	4x10 ³	1x10 ¹
Mean	3x10¹	3x10¹	3x10¹	1x10⁴	3x10⁴	4x10²	9x10³	4x10³	1x10¹
APLC19_1	7x10 ¹	6x10 ¹	8x10 ¹	2x10 ⁴	2x10 ⁴	4x10 ²	1x10 ⁴	4x10 ³	2x10 ¹
APLC19_2	7x10 ¹	5x10 ¹	8x10 ¹	2x10 ⁴	1x10 ⁴	9x10 ²	9x10 ³	8x10 ³	2x10 ¹
APLC20_2	5x10 ¹	2x10 ¹	5x10 ¹	2x10 ⁴	1x10 ⁴	7x10 ²	8x10 ³	4x10 ³	2x10 ¹
Mean	6x10¹	4x10¹	7x10¹	2x10⁴	1x10⁴	6x10²	9x10³	9x10³	2x10¹

On the one hand, samples from El Hierro showed the highest concentration factors, of the order of 10⁴ and 10³, for ²¹⁰Po, ²³⁴Th, ²¹⁰Pb and ²²⁸Th, which are particle-reactive radionuclides. Concentration factors for the conservative radionuclides ²³⁴U, ²³⁵U, ²³⁸U and ⁴⁰K were found lower, of the order of 10¹, while ²²⁶Ra had an intermediate value of the order of 10². On the other hand, for the samples from Las Canteras, the highest values of CFs were also obtained for the particle-reactive radionuclides with an order of magnitude of 10⁴. ⁴⁰K and ²³⁵U had CFs of the same magnitude as the samples of El Hierro, while ²³⁴U, ²³⁸U and ²²⁶Ra, were found one order of magnitude higher. However, these differences are not significantly different as we haven't been able to measure all of the radioisotopes in our water samples. Despite this, the results from Las Canteras agree with the CFs calculated by Tejera et al. (2019) from algae arrivals on Las Canteras beach.

This tendency of the algae to accumulate higher amounts of particle-reactive radionuclides than of conservative radionuclides is a behaviour already known and documented (Tejera et al., 2019) which indicates that algae have a greater affinity for concentrating the particulate phase of seawater than the dissolved phase. This could be explained by the scavenging of the particle-reactive radionuclides that are removed from the dissolved phase and sink in the water column or also because of particle-reactive radionuclides adhering to the algae surface.

3.3 Uranium and Thorium series ratios

Figure 6 shows the ratios calculated between different radionuclides within the same decay series, always plotting the daughter nuclide against the father nuclide of the series. Therefore, for the ^{238}U series we have calculated $^{234}\text{Th}/^{238}\text{U}$, $^{234}\text{U}/^{238}\text{U}$, $^{226}\text{Ra}/^{238}\text{U}$, $^{210}\text{Pb}/^{226}\text{Ra}$ and $^{210}\text{Po}/^{210}\text{Pb}$ ratios, and to compare it with ^{232}Th series we have performed the $^{228}\text{Th}/^{234}\text{Th}$ ratio, as well as the ratio $^{228}\text{Th}/^{226}\text{Ra}$. Moreover, it has been calculated the ratio of $^{235}\text{U}/^{238}\text{U}$ to compare ^{235}U series (Annex I.III) with ^{238}U series.

The values for $^{234}\text{Th}/^{238}\text{U}$ are clearly deviated from the typical ratio found in marine water. Algae tend to accumulate much more thorium than uranium which is explained if thorium, which is much more reactive than uranium, is removed from the dissolved phase by scavenging, thus leaving seawater impoverished in thorium, and gets finally attached to the algae (Tejera et al., 2019). For the ratio of $^{234}\text{U}/^{238}\text{U}$, as both are conservatives, the values for the samples' ratios follow the same equilibrium than in marine water.

The values obtained for the ratio of $^{226}\text{Ra}/^{238}\text{U}$ show a behaviour clearly far from the equilibrium of the seawater, whose value is 0.08, so they are enriched in ^{226}Ra . The values seem to be closer to the equilibrium that usually occurs in the earth's crust. This could be because of a ^{226}Ra discharge from the coast towards the coastal waters through landslides. In the graph where ^{210}Pb is plotted against ^{226}Ra , it can be seen a clear enrichment of algae in ^{210}Pb , a particle-reactive radionuclide, with respect to ^{226}Ra , a conservative particle.

While ^{210}Po and ^{210}Pb , both reactive particles, are found in similar proportions in seawater, we can see that there is a higher concentration of polonium than lead in algae samples, as it has been also seen in previous studies (Tejera et al., 2019). This is due to the preference of lead for the inorganic phase and the preference for polonium for the organic phase, being used as habitual tracers for both phases (Su et al., 2017).

From the $^{228}\text{Th}/^{234}\text{Th}$, which both have the same nature but belong to different decay series, we have obtained higher concentrations in algae of ^{234}Th than of ^{228}Th . Moreover, a different behaviour is observed in the samples from Las Canteras. To better compare both series it is used the ratio $^{228}\text{Th}/^{226}\text{Ra}$, where it is observed that in general the behaviour for the algae is closer to the equilibrium found in earth's crust and slightly closer to the ratio of coastal waters. Algae are enriched in ^{228}Th , a fact that can again be explained by a contribution of ^{228}Ra through landslides and coastal discharge when it rains. In addition, samples from the volcano zone are the ones closer to the ratio of marine water, possibly because they could be enriched in ^{226}Ra due to the underwater eruption.

Finally, due to the low values of ^{235}U it is difficult to say anything about its behaviour.

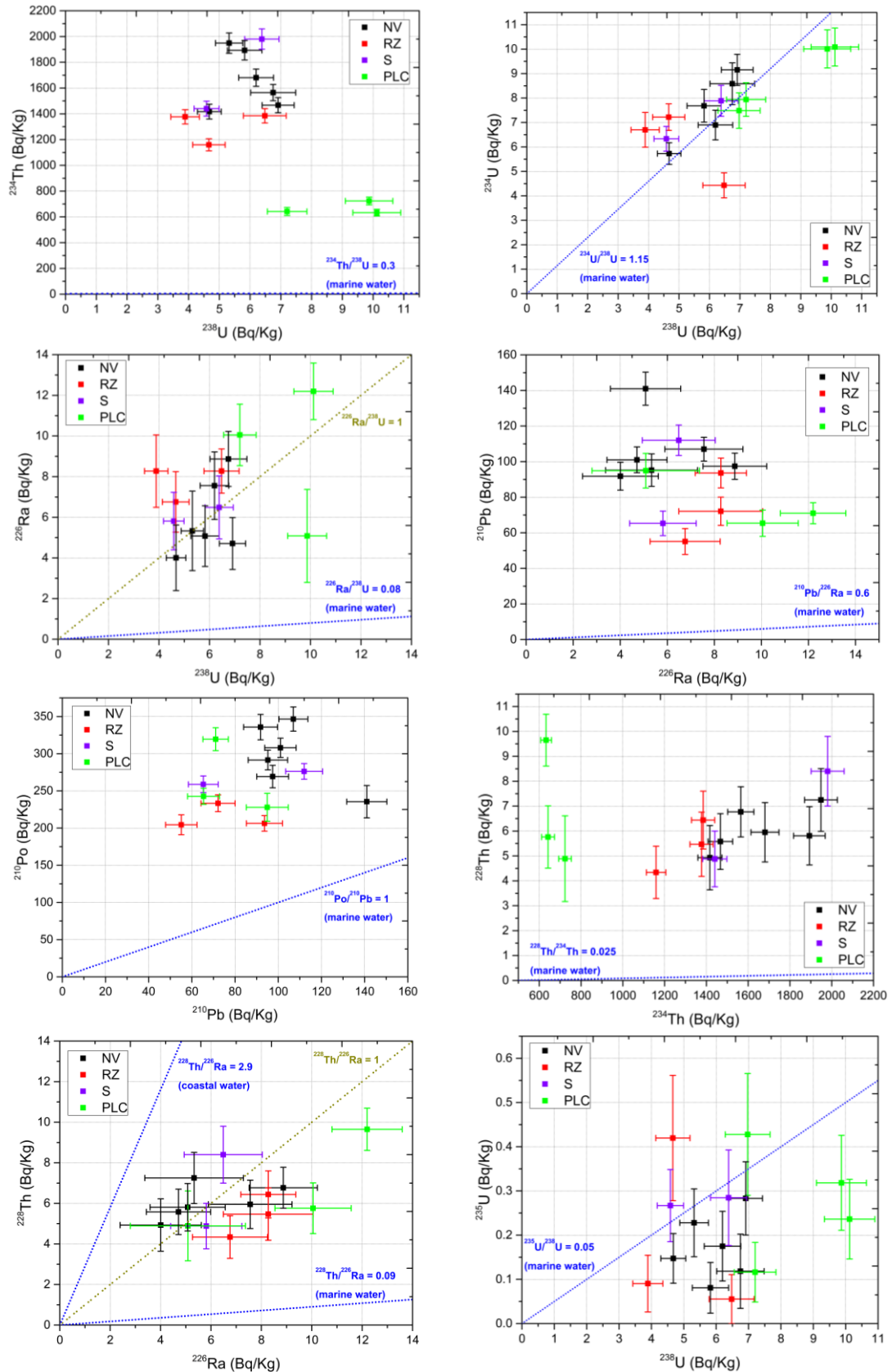


Figure 6. Ratios of $^{234}\text{Th}/^{238}\text{U}$, $^{234}\text{U}/^{238}\text{U}$, $^{226}\text{Ra}/^{238}\text{U}$, $^{210}\text{Pb}/^{226}\text{Ra}$, $^{210}\text{Po}/^{210}\text{Pb}$, $^{228}\text{Th}/^{234}\text{Th}$, $^{228}\text{Th}/^{226}\text{Ra}$ and $^{235}\text{U}/^{238}\text{U}$. Blue and brown dot lines represent the typical values of seawater and earth's crust.

In Table 6, the mean values calculated for each of the ratios and for the different considered areas have been exposed. It can be noticed very significant differences between El Hierro and Las Canteras for the following ratios: $^{234}\text{Th}/^{238}\text{U}$, which has values of 290 ± 30 and 75 ± 7 respectively; $^{228}\text{Th}/^{234}\text{Th}$ with mean ratios of $(3.8 \pm 0.8) \times 10^{-3}$ and $(1.0 \pm 0.2) \times 10^{-2}$, and for $^{238}\text{U}/^{40}\text{K}$, which was calculated in order to compare potassium with the decay series of ^{238}U , and whose values are $(5.1 \pm 0.5) \times 10^{-3}$ and $(7.2 \pm 0.7) \times 10^{-3}$. Additionally, some small differences have been found for the ratios of $^{234}\text{U}/^{238}\text{U}$ between PLC and S areas and for $^{226}\text{Ra}/^{238}\text{U}$ between PLC and RZ areas.

Table 6. Mean values for the calculated ratios for the *L. variegata* radionuclides' activity concentrations for the different considered areas in El Hierro and Las Canteras.

Nuclide	El Hierro			Las Canteras	
	RZ	S	NV	EH Mean	PLC Mean
$^{234}\text{Th}/^{238}\text{U}$	270 ± 30	310 ± 30	290 ± 30	290 ± 30	75 ± 7
$^{234}\text{U}/^{238}\text{U}$	1.20 ± 0.16	1.31 ± 0.13	1.27 ± 0.13	1.26 ± 0.14	1.05 ± 0.10
$^{226}\text{Ra}/^{238}\text{U}$	1.6 ± 0.4	1.1 ± 0.3	1.0 ± 0.3	1.2 ± 0.3	1.0 ± 0.2
$^{210}\text{Pb}/^{226}\text{Ra}$	9 ± 2	14 ± 4	19 ± 6	16 ± 4	10 ± 4
$^{210}\text{Po}/^{210}\text{Pb}$	3.1 ± 0.4	3.2 ± 0.3	2.9 ± 0.3	3.0 ± 0.3	3.5 ± 0.4
$^{228}\text{Th}/^{234}\text{Th}$	$(4.1 \pm 0.9) \times 10^{-3}$	$(3.8 \pm 0.8) \times 10^{-3}$	$(3.7 \pm 0.7) \times 10^{-3}$	$(3.8 \pm 0.8) \times 10^{-3}$	$(1.0 \pm 0.2) \times 10^{-2}$
$^{228}\text{Th}/^{226}\text{Ra}$	0.7 ± 0.2	1.1 ± 0.3	1.1 ± 0.4	1.0 ± 0.3	0.8 ± 0.3
$^{235}\text{U}/^{238}\text{U}$	$(4.1 \pm 1.9) \times 10^{-2}$	$(5.1 \pm 1.8) \times 10^{-2}$	$(2.9 \pm 1.2) \times 10^{-2}$	$(3.6 \pm 1.5) \times 10^{-2}$	$(3.3 \pm 1.2) \times 10^{-2}$
$^{238}\text{U}/^{40}\text{K}$	$(4.5 \pm 0.6) \times 10^{-3}$	$(5.0 \pm 0.5) \times 10^{-3}$	$(5.4 \pm 0.5) \times 10^{-3}$	$(5.1 \pm 0.5) \times 10^{-3}$	$(7.2 \pm 0.7) \times 10^{-3}$

3.4 Statistical analysis

For the statistics to be meaningful, the number of sites in each area has to be balanced. For this reason, the gamma emission radionuclides of six of the new samples from the second campaign (see Table 7) have been included in the two-way ANOVA tests. Las Lapillas (LP1 and LP2) and Punta del Río (PR1 and PR2) are in the zone affected by the volcano, while Tamaduste (TM1 and TM2) is in the unaffected area. It should be noted that it has not been possible to differentiate the stain area due to the lack of sites measured in this area. We are currently working on the pending samples in order to be able to distinguish this area in the study and cover the north coast of the island.

Similarly, in the one-way ANOVAs that were carried out including the samples from Las Canteras, in order to achieve a balance number of sites per area, some samples had to be collapsed. This has allowed as to include in these tests the radionuclides measured through alpha spectrometry and the ratios in which they are involved.

Table 7. Activity concentrations (Bq/Kg) of the gamma emission radionuclides for *L. variegata* samples from the second campaign in El Hierro. Alpha radionuclides have not been yet measured.

Sample	²³⁴ Th	²²⁶ Ra	²¹⁰ Pb	²²⁸ Th	⁴⁰ K
LP1	1150 ± 50	6.1 ± 1.8	79 ± 8	5.5 ± 1.3	680 ± 40
LP2	1350 ± 60	5.5 ± 1.5	79 ± 9	6.0 ± 1.3	800 ± 40
PR1	1410 ± 60	6.9 ± 1.9	114 ± 9	8.2 ± 1.4	1100 ± 50
PR2	1650 ± 70	6.9 ± 1.4	104 ± 8	11.5 ± 1.2	1030 ± 50
TM1	910 ± 40	16.3 ± 1.0	90 ± 7	11.8 ± 1.0	780 ± 40
TM2	1130 ± 50	13.8 ± 1.4	96 ± 8	13.4 ± 1.1	850 ± 40

Table 8 contains the resulting p-values for each of the ANOVA's test performed. The rest of the values obtained for the different parameters of the ANOVAs are all listed in Annex II, tables II.1 and II.2.

Table 8. P-values obtained with ANOVA corresponding to the different variables considered in the comparison between NV and V areas and NV, V and PLC areas. P-values in bold are those below 0.05, while those marked with the asterisk and in blue, those below 0.20.

Variable	NV-V	NV-V-PLC	Variable	NV-V-PLC
⁴⁰ K	0.45	0.027	²³⁴ U	0.11*
²³⁴ Th	0.34	0.0008	²³⁵ U	0.98
²²⁶ Ra	0.014	0.79	²³⁸ U	0.07*
²¹⁰ Pb	0.14*	0.13*	²³⁴ Th/ ²³⁸ U	0.0012
²²⁸ Th	0.11*	0.90	²³⁴ U/ ²³⁸ U	0.031
²¹⁰ Pb/ ²²⁶ Ra	0.19*	0.47	²²⁶ Ra/ ²³⁸ U	0.71
²²⁸ Th/ ²³⁴ Th	0.024	0.08	²¹⁰ Po/ ²¹⁰ Pb	0.40
²²⁸ Th/ ²²⁶ Ra	0.39	0.38	²³⁵ U/ ²³⁸ U	0.53

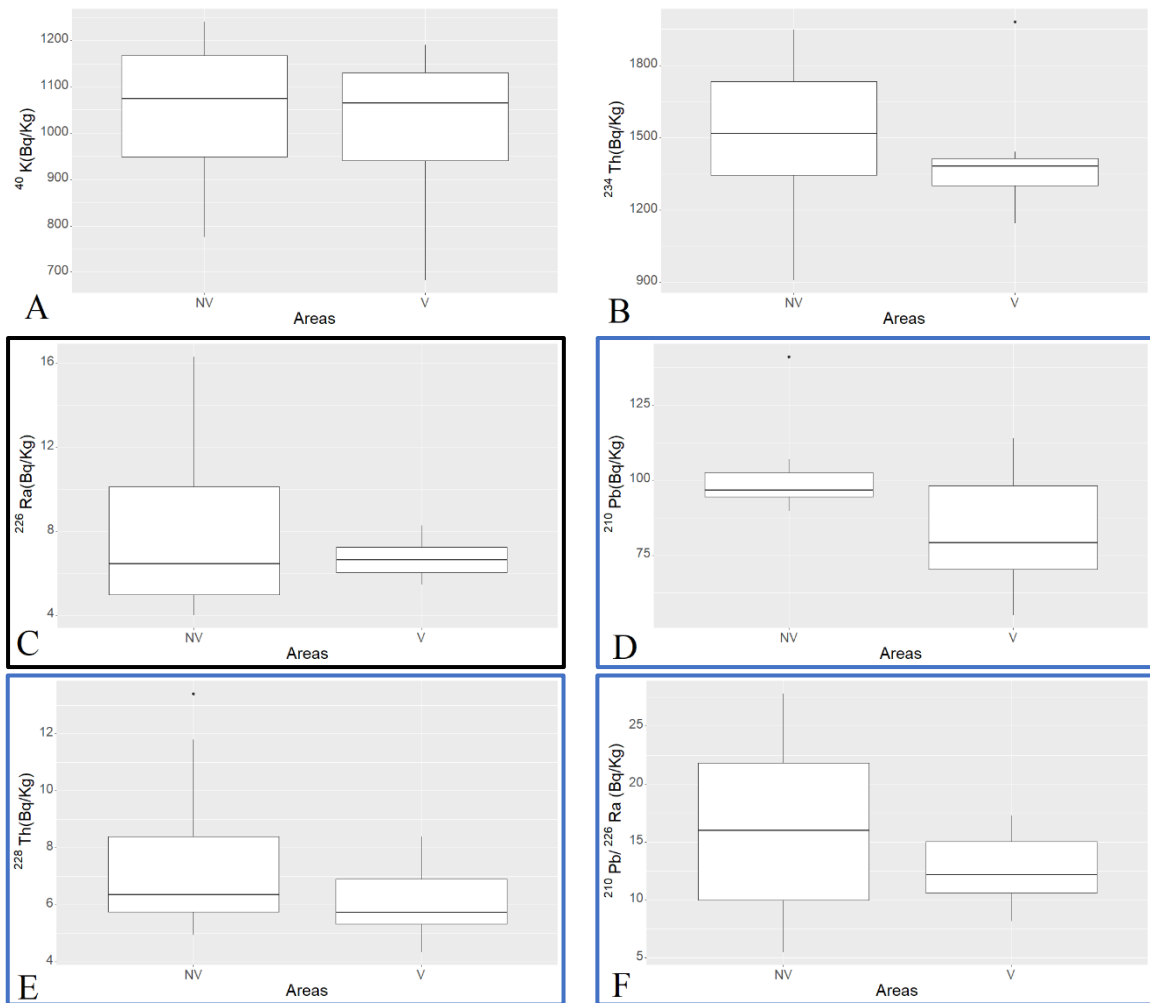
For the ANOVAs testing for differences between the NV and V areas, ⁴⁰K, ²³⁴Th and the ratio ²²⁸Th/²²⁶Ra were found to be similar (Fig. 7 plots **A**, **B** and **H**, and Table 8 for the corresponding variables). Statistically significant differences between the NV and volcanic areas were otherwise found for ²²⁶Ra and ²²⁸Th/²³⁴Th (Fig. 7 plots **C** and **G**, and Table 8 for the corresponding p-values). For ²¹⁰Pb and ²²⁸Th radionuclides, and for the ratio ²¹⁰Pb/²²⁶Ra the differences between the two areas were not statistically significance, probably due to a lack of replication per zone; however, looking at their boxplots (Fig. 7 plots **D**, **E** and **F**) and accepting p-values below 0.20 (Table 8), they could be considered different.

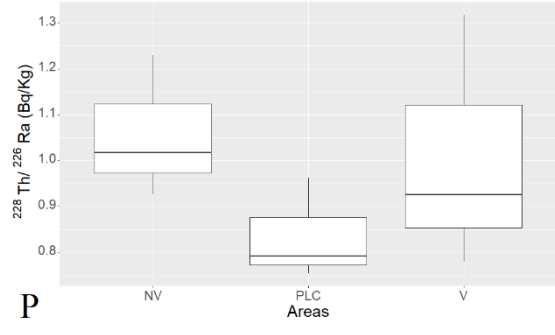
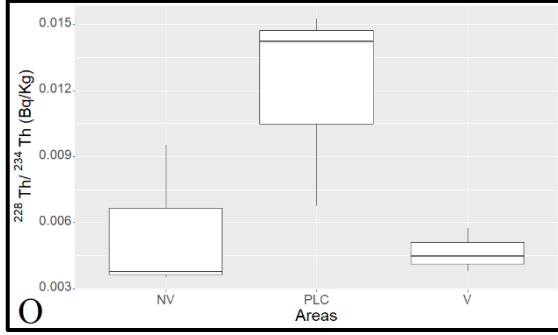
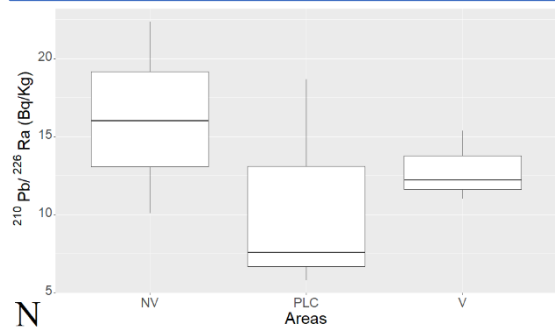
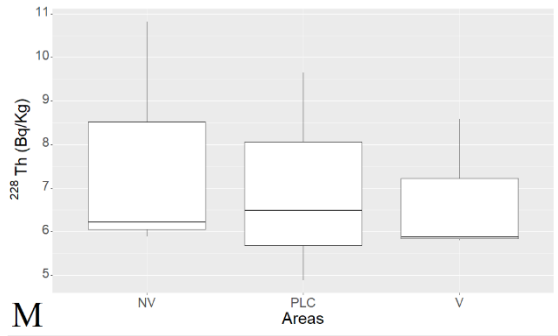
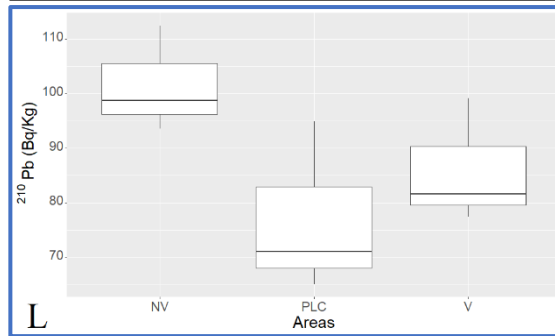
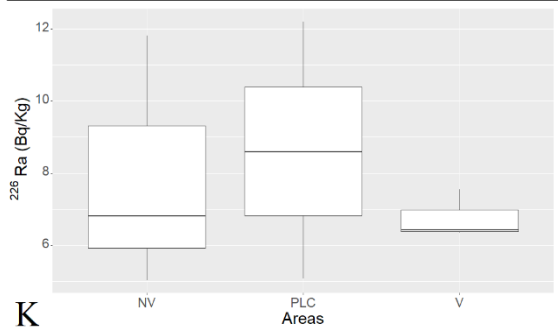
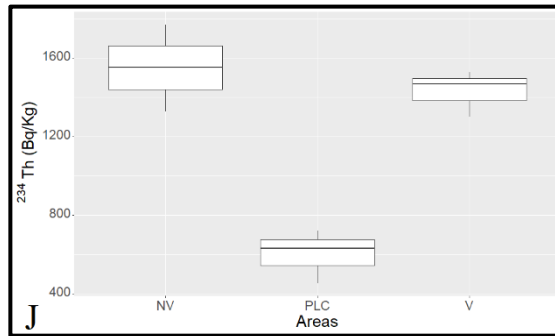
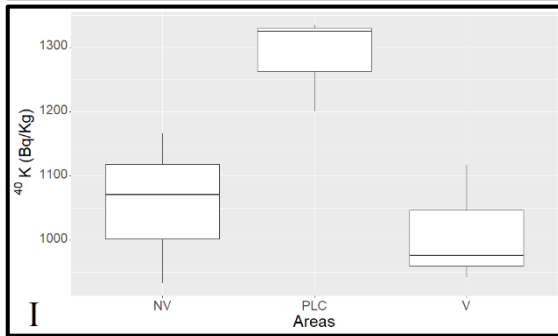
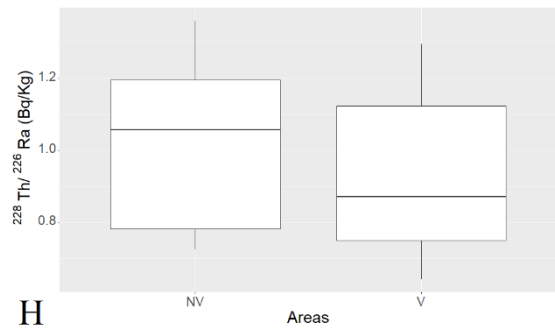
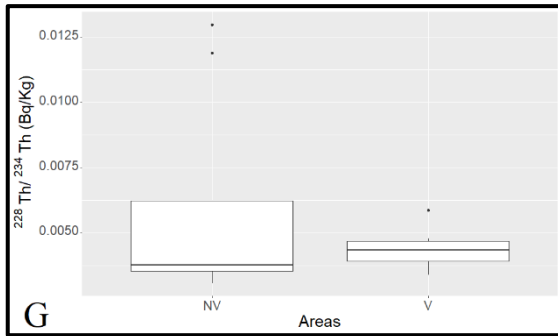
For the one-way ANOVAs testing for differences between the NV, V and PLC areas, similar values were found for ²²⁶Ra, ²²⁸Th, ²¹⁰Pb/²²⁶Ra, ²²⁸Th/²²⁶Ra, ²³⁵U, ²²⁶Ra/²³⁸U, ²¹⁰Po/²¹⁰Pb and ²³⁵U/²³⁸U (Fig. 7 plots **K**, **M**, **N**, **P**, **Q**, **V**, **W** and **X** and Table 8). On the other hand, differences between NV and V and PLC were observed for the radionuclides

^{40}K , ^{234}Th and for the ratios $^{228}\text{Th}/^{234}\text{Th}$, $^{234}\text{Th}/^{238}\text{U}$ and $^{234}\text{U}/^{238}\text{U}$ (Fig. 7 plots **I**, **J**, **O**, **T** and **U** and Table 8). Finally, some differences can be noticed within the areas for ^{210}Pb , ^{234}U and ^{238}U (Fig. 7 plots **L**, **Q** and **S**) with p-values below 0.20 (Table 8).

This statistical analysis has allowed us to see that there is a certain impact in the areas around the volcano eruption, as significant differences have been found with ^{226}Ra , as had already been seen in the previous study of the impact on sediments (Manzanares et al., 2019). In addition, different values were also obtained for $^{228}\text{Th}/^{234}\text{Th}$ ratio between both areas.

When the samples from Las Canteras have been added to the statistical analysis, quite interesting results have also been obtained: both areas greatly differ with the activity concentrations of ^{40}K and ^{234}Th , as well as with the ratios of $^{228}\text{Th}/^{234}\text{Th}$, $^{234}\text{Th}/^{238}\text{U}$ and $^{234}\text{U}/^{238}\text{U}$.





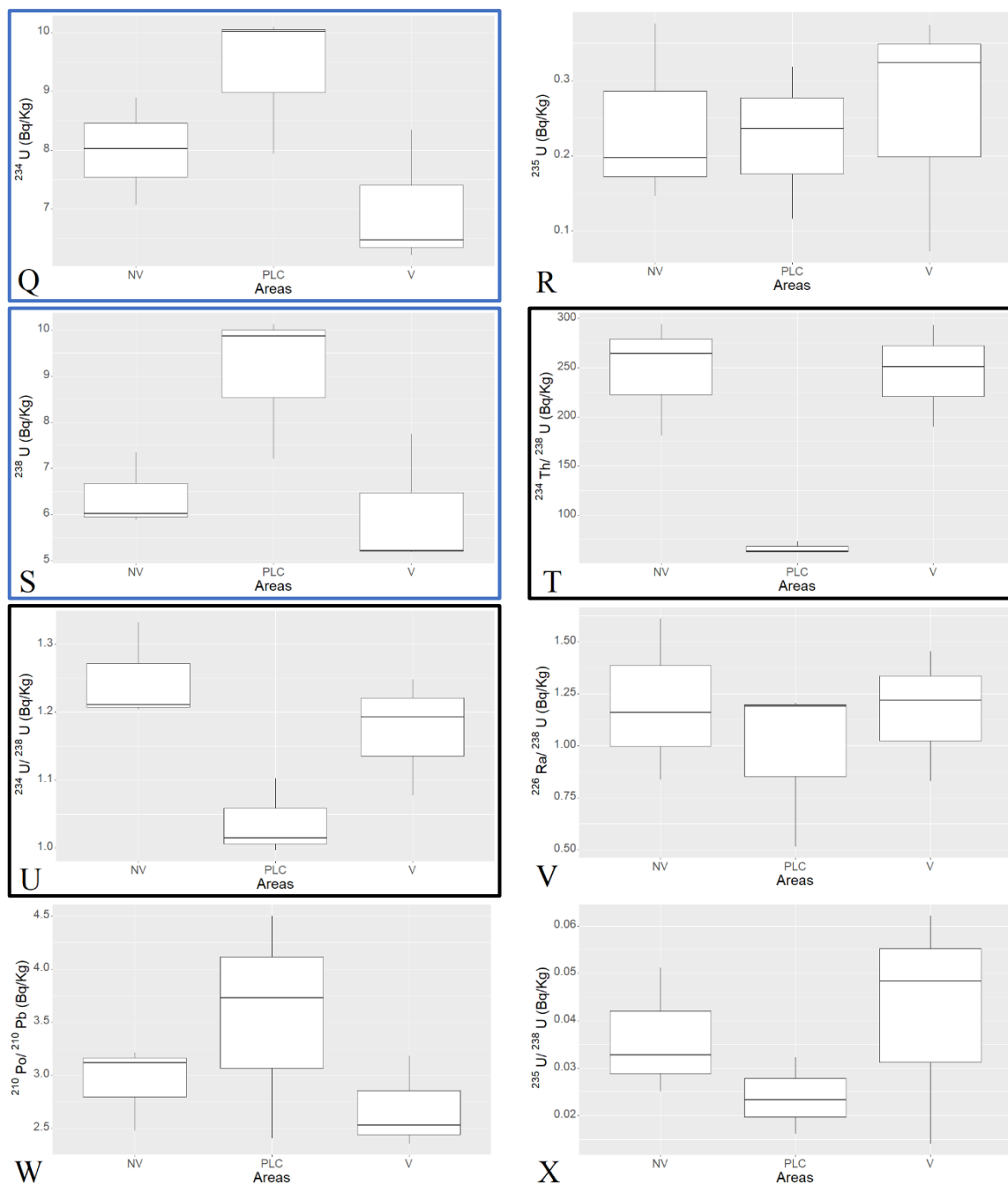


Figure 7. Boxplots for the different activity concentrations and ratios between the NV and V areas and within the NV, V and PLC areas. Those framed in black are the statistically different according to the ANOVAs, while those framed in blue are the ones that we have also considered different with p-values < 0.20.

4. Conclusions

The radiological analysis of the *Lobophora variegata* brown algae, collected in El Hierro island, shows a possible impact of the volcano in the south-western part of the island, causing variations in the activity concentrations of some of the radionuclides measured in algae and seawater samples.

Specifically, activity concentrations of ^{234}Th and ^{210}Pb show higher values in El Hierro than those measured in Las Canteras; however, *L. variegata* from El Hierro have slightly lower activity concentrations of ^{234}U and ^{238}U . In addition, activity concentrations measured of ^{40}K in El Hierro samples are lower than the ones measured in the samples from Las Canteras. Moreover, higher activity concentrations of ^{210}Po have been measured in El Hierro seawater than those measured in Las Canteras. This could be explained if the underwater eruption had caused a considerable increase of radionuclides of ^{238}U natural series, which would justify an increase in the following radioisotopes of the natural decay series. However, for ^{210}Pb values no clear pattern has been observed within areas, as there is a high fluctuation between sites.

With regard to the concentration factors calculated for algae on both islands, it cannot be seen any noticeable difference due to the variations in algae activity concentrations between islands are not large enough to cause a change in the order of magnitude for the concentration factors.

For the ratios calculated among the radionuclides, it has been seen that for those ratios involving conservative radionuclides, the ratios were close to equilibrium, while for those involving non-conservative radionuclides, the ratios were not in equilibrium and in some cases were deviated from the typical values found in marine waters.

Finally, the statistical analysis has revealed significant differences between the non-affected area and the area affected by the volcano with the activity concentrations for ^{226}Ra and the ratio $^{228}\text{Th}/^{234}\text{Th}$. In addition, significant differences have also been obtained between algae sampled in El Hierro Island and those sampled in Las Canteras for ^{40}K , ^{234}Th , $^{228}\text{Th}/^{234}\text{Th}$, $^{234}\text{Th}/^{238}\text{U}$ and $^{234}\text{U}/^{238}\text{U}$.

To conclude, the slightly higher values that through the descriptive analysis were found for ^{226}Ra in the area affected by the volcano, have not been confirmed by the statistical analysis. This could be because of the high activity concentrations of ^{226}Ra in Tamaduste that could be attributable to local characteristics of the sites, such as anthropogenic influences, and not to the volcano.

Increases in some of the radionuclides in ^{238}U series, such as ^{210}Po and ^{234}Th , have been confirmed on El Hierro island, which could be related with the radiological impact of the Tagoro volcano.

Further research is required in order to confirm above mentioned conclusions, as well as to understand other results, such as the low activity concentrations of ^{40}K measured in El Hierro compared to that measured in Las Canteras.

Acknowledgments

I would like to thank my advisors Dra. Alicia M. Tejera Cruz, Dr. Pablo Martel Escobar and Dr. Fernando J. Tuya Cortés for guiding and supervising this project, without their help and advice it wouldn't have been possible. I would also like to thank Armando del Rosario Pinilla for agreeing to collaborate in this project by collecting the samples of the second campaign. Finally, I thank my colleague Daniel Santana Toscano for participating in the first campaign in El Hierro and for his encouragement throughout the hole period, as well as all the people who personally and academically have supported me.

5. References

- Aarkrog, A. (2003). Input of anthropogenic radionuclides into the World Ocean. *Deep-Sea Research Part II: Topical Studies in Oceanography*, 50(17–21), 2597–2606. [https://doi.org/10.1016/S0967-0645\(03\)00137-1](https://doi.org/10.1016/S0967-0645(03)00137-1)
- Alonso, H., Cruz-Fuentes, T., Rubiano, J. G., González-Guerra, J., Cabrera, C., Arnedo, M. A., Tejera, A., Rodríguez-González, A., P-erez-Torrado, F.J., Martel, P. (2015). Radon in Groundwater of the Northeastern Gran Canaria Aquifer. 2575–2590. <https://doi.org/10.3390/w7062575>
- Arnedo, M. A. (2014). Evaluación del fondo radiactivo natural de las Islas Canarias Orientales, implicaciones radiológicas sobre la población.
- Arnedo, M. A., Rubiano, J. G., Alonso, H., Tejera, A., González, A., González, J., Gil, J.M., Rodríguez, R., Martel, P., Bolivar, J. P. (2017). Mapping natural radioactivity of soils in the eastern Canary Islands. *Journal of Environmental Radioactivity*, 166, 242–258. <https://doi.org/10.1016/j.jenvrad.2016.07.010>
- Arnedo, M. A., Tejera, A., Rubiano, J. G., Alonso, H., Gil, J. M., Rodríguez, R., & Martel, P. (2013). Natural radioactivity measurements of beach sands in gran Canaria, Canary Islands (Spain). *Radiation Protection Dosimetry*, 156(1), 75–86. <https://doi.org/10.1093/rpd/nct044>
- Baltas, H., Kiris, E., & Sirin, M. (2017). Determination of radioactivity levels and heavy metal concentrations in seawater, sediment and anchovy (*Engraulis encrasicolus*) from the Black Sea in Rize, Turkey. *Marine Pollution Bulletin*, 116(1–2), 528–533. <https://doi.org/10.1016/j.marpolbul.2017.01.016>
- Belivermiş, M., Kılıç, Ö., Efe, E., Sezer, N., Gönülal, O., & Arslan Kaya, T. N. (2019). Mercury and Po-210 in mollusc species in the island of Gökçeada in the north-eastern Aegean Sea: Bioaccumulation and risk assessment for human consumers. *Chemosphere*, 235, 876–884. <https://doi.org/10.1016/j.chemosphere.2019.06.214>
- Betancor, S., Tuya, F., Gil-Díaz, T., Figueroa, F. L., & Haroun, R. (2014). Effects of a submarine eruption on the performance of two brown seaweeds. *Journal of Sea Research*, 87, 68–78. <https://doi.org/10.1016/j.seares.2013.09.008>
- Blasco, M., Gázquez, M. J., Pérez-Moreno, S. M., Grande, J. A., Valente, T., Santisteban, M., de la Torre, M.L., Bolívar, J. P. (2016). Polonium behaviour in reservoirs potentially affected by acid mine drainage (AMD) in the Iberian Pyrite Belt (SW of Spain). *Journal of Environmental Radioactivity*, 152, 60–69. <https://doi.org/10.1016/j.jenvrad.2015.11.008>
- Buesseler, K. O., Pike, S., Maiti, K., Lamborg, C. H., Siegel, D. A., & Trull, T. W. (2009). Thorium-234 as a tracer of spatial, temporal and vertical variability in particle flux in the

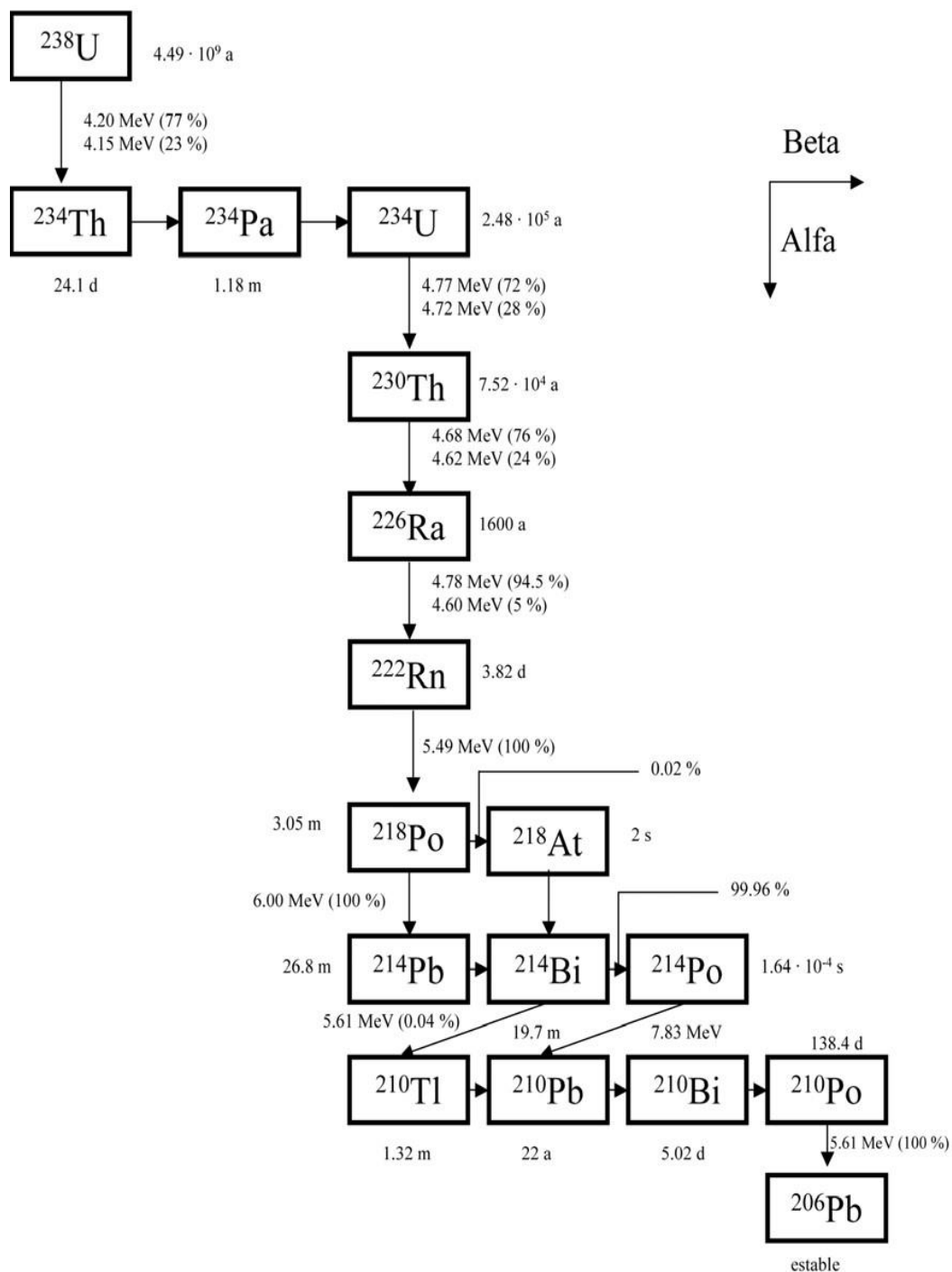
- North Pacific. *Deep-Sea Research Part I*, 56(7), 1143–1167. <https://doi.org/10.1016/j.dsr.2009.04.001>
- Burnett, W. C., Peterson, R., Moore, W. S., & de Oliveira, J. (2008). Radon and radium isotopes as tracers of submarine groundwater discharge-Results from the Ubatuba , Brazil SGD assessment intercomparison. *76*, 501–511. <https://doi.org/10.1016/j.ecss.2007.07.027>
- Canberra. (2017). Alpha Analyst: Integrated Alpha Spectrometer.
- Carracedo, J. C., Perez-Torrado, F. J., Rodriguez-Gonzalez, A., Fernandez-Turiel, J. L., Klügel, A., Troll, V. R., & Wiesmaier, S. (2012). The ongoing volcanic eruption of El Hierro, Canary Islands. *Eos*, 93(9), 89–90. <https://doi.org/10.1029/2012EO090002>
- Cetnar, J. (2006). General solution of Bateman equations for nuclear transmutations. *Annals of Nuclear Energy*, 33(7), 640–645. <https://doi.org/10.1016/j.anucene.2006.02.004>
- Chakraborty, S., Bhattacharya, T., Singh, G., & Maity, J. P. (2014). Benthic macroalgae as biological indicators of heavy metal pollution in the marine environments: A biomonitoring approach for pollution assessment. *Ecotoxicology and Environmental Safety*, 100(1), 61–68. <https://doi.org/10.1016/j.ecoenv.2013.12.003>
- Cockenpot, S., Claude, C., & Radakovitch, O. (2015). Estimation of air-water gas exchange coefficient in a shallow lagoon based on ²²²Rn mass balance. *Journal of Environmental Radioactivity*, 143, 58–69. <https://doi.org/10.1016/j.jenvrad.2015.02.007>
- Eugenio, F., Martin, J., Marcello, J., & Fraile-Nuez, E. (2014). Environmental monitoring of El Hierro Island submarine volcano, by combining low and high resolution satellite imagery. *International Journal of Applied Earth Observation and Geoinformation*, 29(1), 53–66. <https://doi.org/10.1016/j.jag.2013.12.009>
- Fowler, S. W. (2011). ²¹⁰Po in the marine environment with emphasis on its behaviour within the biosphere. *Journal of Environmental Radioactivity*, 102(5), 448–461. <https://doi.org/10.1016/j.jenvrad.2010.10.008>
- Garzón Ruiperez, L. (1979). Radiactividad y medioambiente. Retrieved from <http://search.ebscohost.com/login.aspx?direct=true&db=cat07429a&AN=ulpgc.110521&site=eds-live>
- Hierro, A., Bolivar, J. P., Vaca, F., & Borrego, J. (2012). Behavior of natural radionuclides in surficial sediments from an estuary impacted by acid mine discharge and industrial effluents in Southwest Spain. *Journal of Environmental Radioactivity*, 110, 13–23. <https://doi.org/10.1016/j.jenvrad.2012.01.005>
- International Atomic Energy Agency. (2010). HELCOM-MORS Proficiency Test Determination of Radionuclides in Fish Flesh Sample. *Analytical Quality in Nuclear Applications*, (13). Retrieved from https://www-pub.iaea.org/MTCD/publications/PDF/IAEA-AQ-13_web.pdf
- Kim, S. H., Lee, H., Lee, S. H., & Kim, I. (2019). Distribution and accumulation of artificial radionuclides in marine products around Korean Peninsula. *Marine Pollution Bulletin*, 146(July), 521–531. <https://doi.org/10.1016/j.marpolbul.2019.06.082>
- Knoll, G. F. (2000). Radiation Detection and Measurement. <https://doi.org/10.1002/hep.22108>
- Lerner, P., Marchal, O., Lam, P. J., & Solow, A. (2018). Effects of particle composition on thorium scavenging in the North Atlantic. *Geochimica et Cosmochimica Acta*, 233, 115–134. <https://doi.org/10.1016/j.gca.2018.04.035>
- Livingston, H. D. (2005). Radioactivity in the Environment: Marine Radioactivity. *Statewide Agricultural Land Use Baseline 2015, 1*. <https://doi.org/10.1017/CBO9781107415324.004>

- Manzanares Obispo, B., Martel Escobar, P., & Tejera Cruz, A. M. (2019). Temporal assessment of the Tagoro volcano radiological impact by mean coastal sediments gamma spectrometry.
- Mouloud Lehitani, H. (2012). Determinación de isótopos de uranio y torio en muestras ambientales por espectrometría alfa: solución de problemas metodológicos y aplicaciones medioambientales.
- Oliveira, J. M., & Carvalho, F. P. (2006). Sequential extraction procedure for determination of uranium, thorium, radium, lead and polonium radionuclides by alpha spectrometry in environmental samples. *Czechoslovak Journal of Physics*, 56(1), D545–D555. <https://doi.org/10.1007/s10582-006-1064-8>
- Padilla, G. D., Hernández, P. A., Padrón, E., Barrancos, J., Pérez, N. M., Melián, G., Nolasco, D., Samara, D., Rodríguez, F., Calvo, D., Hernández, I. (2013). Soil gas radon emissions and volcanic activity at El Hierro (Canary Islands): The 2011-2012 submarine eruption. *Geochemistry, Geophysics, Geosystems*, 14(2), 432–447. <https://doi.org/10.1029/2012GC004375>
- Pham, M. K., Benmansour, M., Carvalho, F. P., Chamizo, E., Degering, D., Engeler, C., Gascó, C., Gwynn, J.P., Harms, A.V., Hrncsek, E., Ibanez, F.L., Ilchmann, C., Ikaheimonen, T., Kanisch, G., Kloster, M., Llaurodo, M., Mairing, A., Møller, B., Morimoto, T., Nielsen, S.P., Nies, H., Norrlid, L.D.R., Pettersson, H.B.L., Povinec, P.P., Rieth, U., Samuelsson, C., Schikowski, J., Šilobritiene, B.V., Smedley, P.A., Suplinska, M., Vartti, V.-P., Vasileva, E., Wong, J., Zalewska, T., Zhou, W. (2014). Certified Reference Material IAEA-446 for radionuclides in Baltic Sea seaweed. *Applied Radiation and Isotopes*, 87, 468–474. <https://doi.org/10.1016/j.apradiso.2013.11.013>
- Praveen Pole, R. P., Feroz Khan, M., & Godwin Wesley, S. (2017). Occurrence of ²¹⁰Po in marine macroalgae inhabiting a coastal nuclear zone, southeast coast of India. *Journal of Environmental Radioactivity*, 169–170, 122–130. <https://doi.org/10.1016/j.jenvrad.2017.01.013>
- Santana-Casiano, J. M., González-Dávila, M., Fraile-Nuez, E., De Armas, D., González, A. G., Domínguez-Yanes, J. F., & Escánez, J. (2013). The natural ocean acidification and fertilization event caused by the submarine eruption of El Hierro. *Scientific Reports*, 3, 1–9. <https://doi.org/10.1038/srep01140>
- Su, K., Du, J., Baskaran, M., & Zhang, J. (2017). Pb disequilibrium at the PN section in the East China Sea. *Journal of Environmental Radioactivity*, 174, 54–65. <https://doi.org/10.1016/j.jenvrad.2016.07.031>
- Tejera, A., Pérez-Sánchez, L., Guerra, G., Arriola-Velásquez, A. C., Alonso, H., Arnedo, M. A., Rubiano, G., Martel, P. (2019). Natural radioactivity in algae arrivals on the Canary coast and dosimetry assessment. *Science of the Total Environment*, 658, 122–131. <https://doi.org/10.1016/j.scitotenv.2018.12.140>
- Tuya, F., & Haroun, R. J. (2006). Spatial patterns and response to wave exposure of shallow water algal assemblages across the Canarian Archipelago: A multi-scaled approach. *Marine Ecology Progress Series*, 311, 15–28. <https://doi.org/10.3354/meps311015>
- Uddin, S., Bebehani, M., Sajid, S., & Karam, Q. (2019). Concentration of ²¹⁰Po and ²¹⁰Pb in macroalgae from the northern Gulf. *Marine Pollution Bulletin*, 145(June), 474–479. <https://doi.org/10.1016/j.marpolbul.2019.06.056>
- UNSCEAR. (2000). Sources and Effects of Ionizing Radiation, United Nations Scientific Committee on the Effects of Atomic Radiation UNSCEAR 2000 Report to the General Assembly, with Scientific Annexes. In *UNSCEAR 2000 Report*. <https://doi.org/10.1097/00004032-199907000-00007>

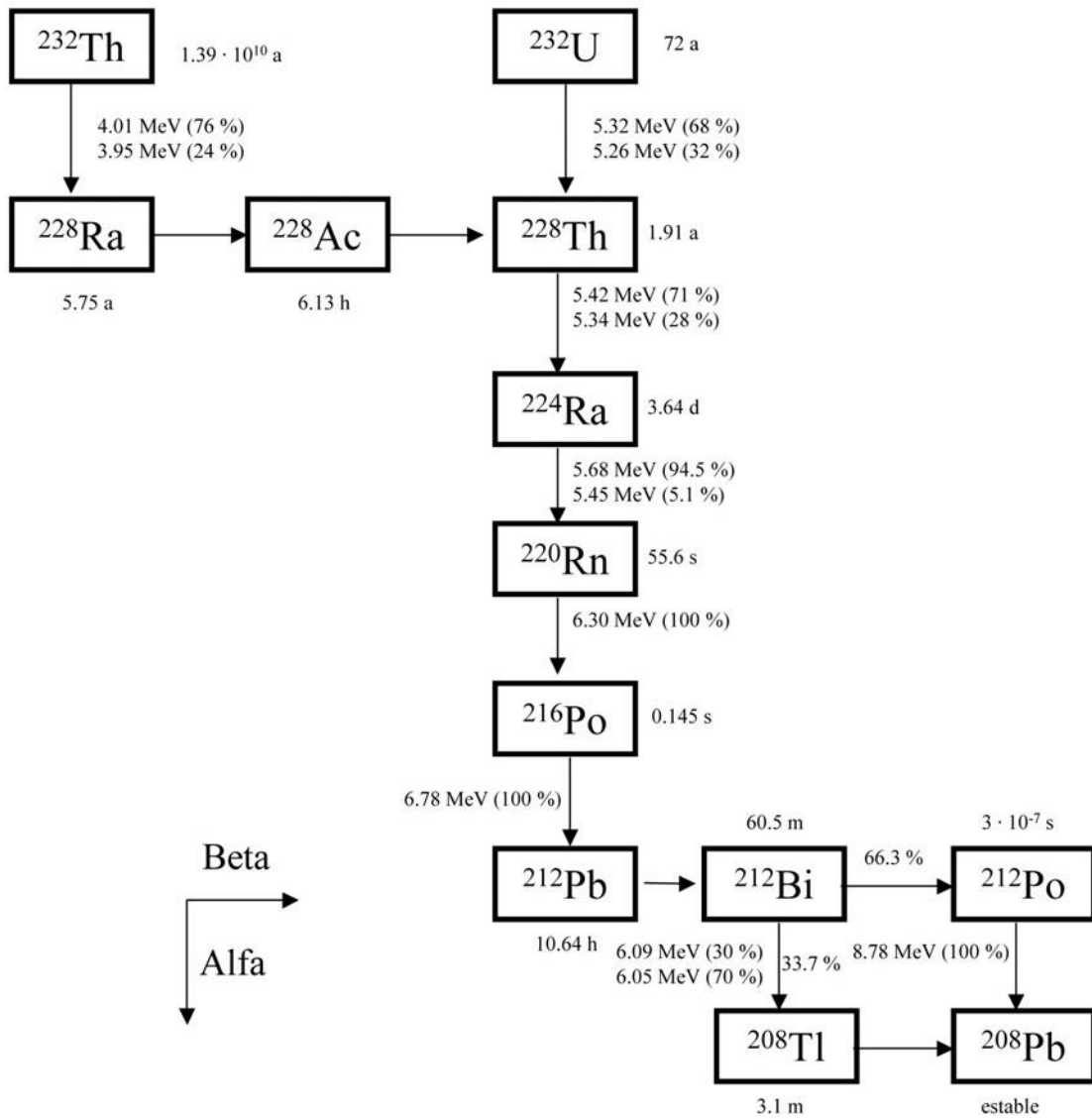
Urgeles, R., Canals, M., Baraza, J., Alonso, B., & Masson, D. (1997). The most recent megalandslides of the Canary Islands: El Golfo debris avalanche and Canary debris flow, west El Hierro Island. *Journal of Geophysical Research: Solid Earth*, 102(B9), 20305–20323. <https://doi.org/10.1029/97jb00649>

Annex I – Radioactive decay series

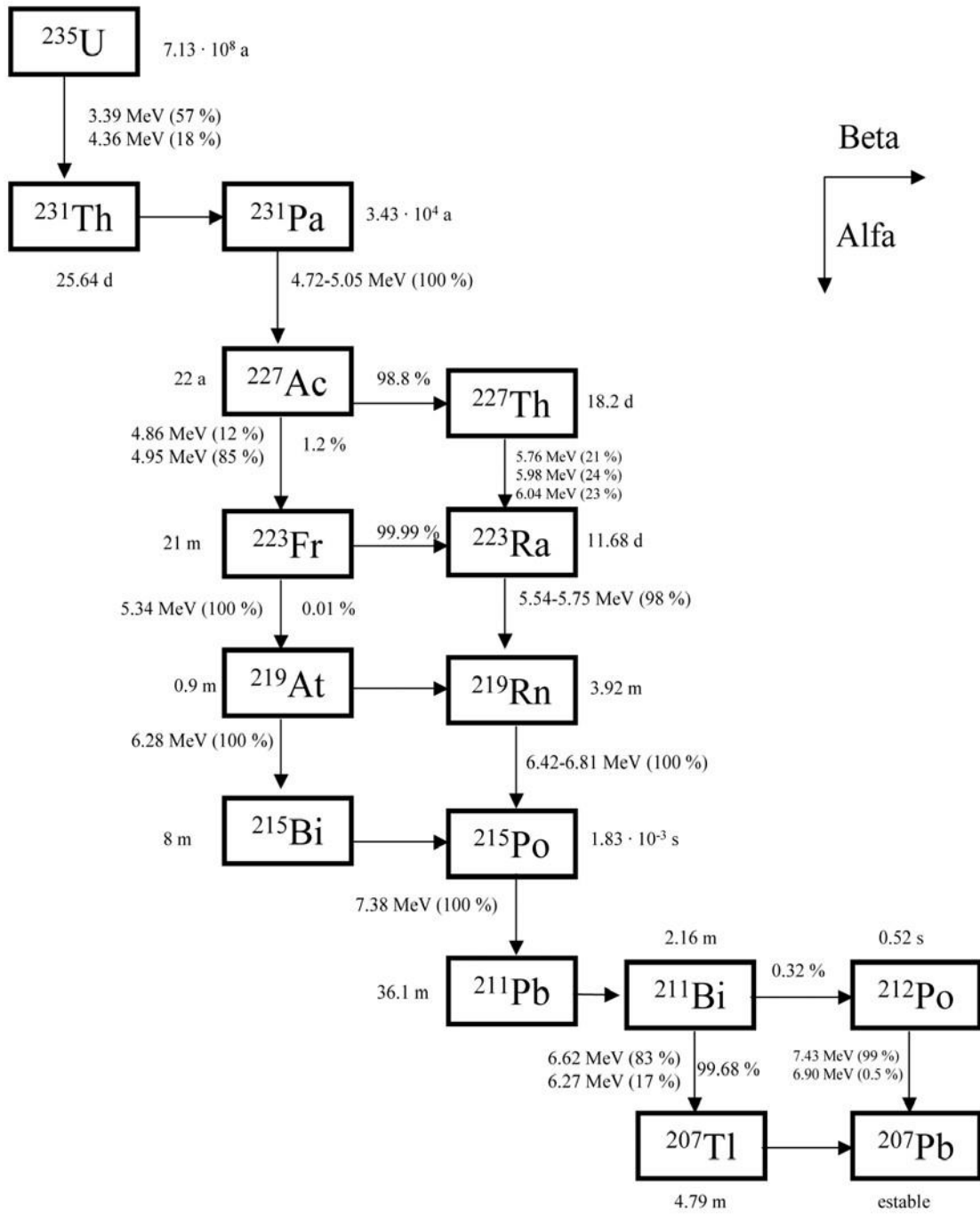
I.I. Natural radioactive decay series of ^{238}U



I.II Natural radioactive decay series of ^{232}Th



I.III. Natural radioactive decay series of ^{235}U



Annex II

Table A.II.1 and Table A.II.2 show the results of one-way and two-way ANOVAs testing for differences in the radionuclides' activity concentrations and the activity concentration ratios, between the areas and sites within each area

Table II.1. Results obtained for the two-way ANOVAs.

Sample	⁴⁰ K			²³⁴ Th		
	Mean Sq	F value	Pr (>F)	Mean Sq	F value	Pr (>F)
Area	4091	0.6249	0.4520	5.075	1.0446	0.3367
Sites	60938	9.3089	0.0030	32.560	6.7016	0.0086
Residuals	6546			4.859		
Sample	²²⁶ Ra			²¹⁰ Pb		
	Mean Sq	F value	Pr (>F)	Mean Sq	F value	Pr (>F)
Area	0.1369	9.8762	0.0138	4.0113	2.7562	0.1355
Sites	0.6909	49.8477	6.24x10 ⁻⁶	0.3040	0.2089	0.9639
Residuals	0.0139			1.4554		
Sample	²²⁸ Th			²¹⁰ Pb/ ²²⁶ Ra		
	Mean Sq	F value	Pr (>F)	Mean Sq	F value	Pr (>F)
Area	0.2747	3.3224	0.1058	0.4919	2.1068	0.1847
Sites	0.3169	3.8336	0.0420	1.2386	5.3049	0.0172
Residuals	0.0827			0.2335		
Sample	²²⁸ Th/ ²³⁴ Th			²²⁸ Th/ ²²⁶ Ra		
	Mean Sq	F value	Pr (>F)	Mean Sq	F value	Pr (>F)
Area	0.00020	7.7852	0.0236	0.0353	0.8343	0.3877
Sites	0.00067	25.4168	8.535x10 ⁻⁵	0.0823	1.9457	0.1885
Residuals	0.00003			0.42316		

Table 9. Results obtained for one-way ANOVAs.

Sample	⁴⁰ K			²³⁴ Th		
	Mean Sq	F value	Pr (>F)	Mean Sq	F value	Pr (>F)
Area	65136	6.9832	0.0274	798437	26.638	0.00078
Residuals	9328			26940		
Sample	²²⁶ Ra			²¹⁰ Pb		
	Mean Sq	F value	Pr (>F)	Mean Sq	F value	Pr (>F)
Area	0.0643	0.2494	0.787	463.13	2.9205	0.1301
Residuals	0.2579			158.58		
Sample	²²⁸ Th			²¹⁰ Pb/ ²²⁶ Ra		
	Mean Sq	F value	Pr (>F)	Mean Sq	F value	Pr (>F)
Area	0.0183	0.1048	0.9021	0.4892	0.8467	0.4743
Residuals	0.1743			0.5777		

Sample	$^{228}\text{Th}/^{234}\text{Th}$			$^{228}\text{Th}/^{226}\text{Ra}$		
	Mean Sq	F value	Pr (>F)	Mean Sq	F value	Pr (>F)
Area	0.0015	4.2261	0.0716	0.0105	1.1422	0.3799
Residuals	0.0003			0.0092		
Sample	^{234}U			^{235}U		
	Mean Sq	F value	Pr (>F)	Mean Sq	F value	Pr (>F)
Area	4.1365	3.4059	0.1027	0.0003	0.0164	0.9838
Residuals	1.2145			0.0205		
Sample	^{238}U			$^{234}\text{Th}/^{238}\text{U}$		
	Mean Sq	F value	Pr (>F)	Mean Sq	F value	Pr (>F)
Area	0.2698	4.3806	0.0672	55.685	24.983	0.0012
Residuals	0.0616			2.229		
Sample	$^{234}\text{U}/^{238}\text{U}$			$^{226}\text{Ra}/^{238}\text{U}$		
	Mean Sq	F value	Pr (>F)	Mean Sq	F value	Pr (>F)
Area	0.0075	6.5951	0.0306	0.0125	0.3709	0.7049
Residuals	0.0011			0.0338		
Sample	$^{210}\text{Po}/^{210}\text{Pb}$			$^{235}\text{U}/^{238}\text{U}$		
	Mean Sq	F value	Pr (>F)	Mean Sq	F value	Pr (>F)
Area	0.0418	1.0803	0.3974	0.0016	0.7136	0.5272
Residuals	0.0387			0.0022		